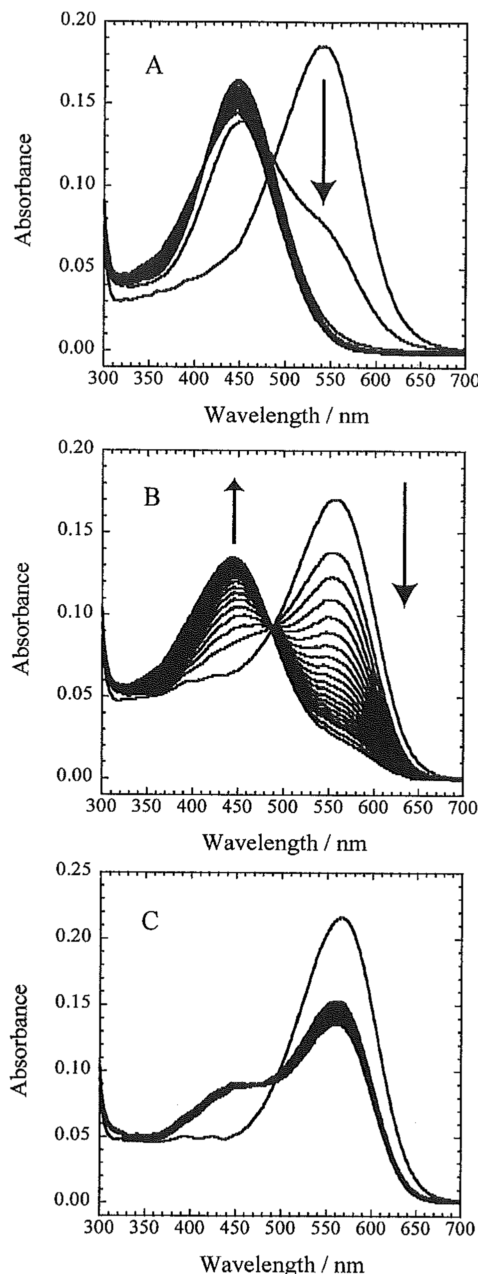

FIGURE 7: Change in the absorption spectra of NpHR during the bleaching reaction by the addition of 50 mM OG at pH 1.5. The concentrations of NaCl were 0 mM (A), 32 mM (B), and 256 mM (C). The first spectrum obtained before the addition of OG, the second spectrum obtasined after the addition of OG at 30 s, and the following spectra obtained in 5-min intervals until 1 h are shown. The final solution in the sample contained 50 mM OG, 2 mM DM, and 10 mM 6-Mix buffer. The pH was adjusted with H_2SO_4.

When the pH is changed from 7 to 1.5, the λ_{max} of chloride-free NpHR largely blue-shifted from 600 to 542 nm (Figure 7A). This absorbance at a low pH remained stable for at least 2 h. The addition of 50 mM OG to the chloride-free NpHR at the low pH induced a rapid decrease in absorbance at the λ_{max} (542 nm) and a subsequent increase in absorption at 450 nm as well as the appearance of absorption (450 nm) at a neutral pH. Similarly, the rate of increase at 450 nm was reduced by the presence of the chloride anion (parts A–C of Figure 7). However, it was clear that the production of acidic I_{450} was strongly inhibited, which was in contrast to the transient formation of I_{450} of the chloride-free NpHR at a neutral pH (Figure 2), suggesting that the bleaching process that occurs between I_{450} and I_{380} may be inhibited by the protonation of NpHR. When the acidic I_{450} was neutralized in the absence of chloride, the recovery of $NpHR^{blue}$ (600 nm) and the formation of I_{380} were observed at the same time.

Table 1: Ratio of the Retinal Isomer Compositions of Several Samples during the Bleaching Process by the Addition of OG in the Dark

sample	retinal isomer composition (%)		
	retinaloxime forms[a]		
	all-*trans*	13-*cis*	retinal forms[a]
$NpHR^{blue}$ (NaCl free)	89	9	2
I_{450} (50 s)[b]	87	10	3
yellow species (30 min)[b]	57	9	35
yellow species (3 h)[b]	43	9	49

[a] Retinaloxime and retinal forms were extracted in the dark with and without hydroxylamine by the denaturation treatment with organic solvent (see the Materials and Methods). [b] Incubation time with 50 mM OG.

Isomerization and Binding of the Retinal to the Protein. The retinal isomer composition of various NpHR samples was analyzed using HPLC; the results are shown in Table 1. The retinaloximes were produced by the cleavage of Schiff-base bonds by the reaction with hydroxylamine (*30–33*). Four isomers of retinaloximes identified as all-*trans* (15-*syn*, 15-*anti*) and 13-*cis* (15-*syn*, 15-*anti*) were detected. Four similar isomers have been detected when the retinal was cleaved from *pharaonis* phoborhodopsin (*33*). The HPLC elution pattern of these retinaloximes extracted from chloride-free $NpHR^{blue}$ was similar to that of NpHR in the presence of NaCl. After the addition of 50 mM OG to the chloride-free $NpHR^{blue}$ for 0, 50 s, 30 min, and 3 h, retinal cleavage and an extraction treatment were carried out. These incubation times corresponded to those of $NpHR^{blue}$, I_{450}, at the initial stage of the yellow species (380 nm pigment) and to the latter stages of the yellow species (380 nm pigment), respectively. As shown in Table 1, the composition of the retinal isomers of $NpHR^{blue}$ and I_{450} did not change. This provided evidence that the large blue shift of λ_{max} from 600 to 450 nm in the dark was not the result of the isomerization of the retinal, e.g., in the case of the 9-*cis* configuration, which has been detected in deionized bR in a pink membrane under continuous illumination (*34*). Similarly, retinaloximes were extracted from the I_{450} trapped at a low pH, suggesting that the retinal isomerization of acidic I_{450} in the dark and its covalent binding as a Schiff base are similar to those of the native structure (data not shown). In contrast, the yellow species exhibited fewer all-*trans* retinaloxime forms and more nonretinaloxime forms, i.e., when extracted from NpHR samples without hydroxylamine using only the organic solvent with incubation time, which might be attributed to the presence of the free retinal.

DISCUSSION

Bacteriorhodopsin and halorhodopsin exhibit two-dimensional crystal packing in the lipidic phase. The crystal structure of *Halobacterium salinarum* HR (HsHR), which

is highly homologous to the NpHR used in the present study, has a trimeric structure as the fundamental assembling unit (*11*). In the present study, active recombinant NpHR was successfully expressed in *E. coli* cells and was purified in the solubilization state with a mild detergent, *n*-dodecyl-β-D-maltopyranoside (DM). The apparent molecular weight of the DM−NpHR estimated by gel-filtration chromatography was 340 kDa, suggesting the assemblage of NpHR monomers in the DM micelles. Using the apparent molecular weight of DM−NpHR, the association number of NpHR monomers contained in a single complex was estimated by various methods. The molecular weight of the NpHR monomer is 32 000 Da according to ESI mass spectrometry (*14*). Using this value, the number of NpHR monomers was calculated to be 10.6. The molecular weight of a single DM micelle is 75 600 Da, and the aggregation number of DM is 148 (*35*). If the DM−NpHR complex were to be assembled together as one DM micelle, the number of NpHR monomers would be expected to be 8.3, although it is difficult to estimate the accurate amount of the DM complex. It is known that the visible CD spectrum of NpHR solubilized with DM detergent indicates a bilobe pattern because of the intermolecular exciton coupling of NpHRs (*15*, *28*). On the other hand, discrete decreases in light scattering at the initial stage of OG mixing were observed (Figure 2). Similarly, it has been reported that solubilized HsHR obtained from the *H. salinarum* membrane has a single positive CD band in the visible region when 0.5% OG is used (*36*). These findings additionally suggest a decrease in the association number of NpHR monomers in the OG micelle system.

The present study was the first to demonstrate, as based on the resolubilization of the DM−NpHR by the addition of OG detergent, that the chloride-free NpHR^{blue} species (600 nm) bleached to the yellow species (I_{380}) by way of an intermediate (I_{450}) at neutral pH. However, the formation of intermediate I_{450} was strongly inhibited by the chloride-binding of NpHR, and yellow species I_{380} was also blocked by the protonation of NpHR. The distribution of the released retinal in the OG-resolubilized NpHR was identified using extraction with an organic solvent and cleavage of the Schiff base by reaction with hydroxylamine. In the absence of chloride, the ratio of the free retinal increased during the last half of the bleaching process (Table 1), which was released from the Schiff base of NpHR. However, the intermediate species (I_{450}), which was generated transiently at a neutral pH, did not lead to an increase in free retinals released from the Schiff base. In addition, the all-*trans*/13-*cis* isomerization ratio before and after the resolubilization of NpHR by the addition of OG detergent was the same.

The bleaching and retinal binding of bR has been reported under both dark and light conditions. In the case of photobleaching of the purple membrane by OG detergent, the primary absorbance showed a direct change to a yellow species (380 nm); moreover, the structural intermediate with a λ_{max} of approximately 450 nm was not observed (*24*). On the other hand, under dark conditions, the structural intermediate of bR, I_{440}, has been observed during the denaturation process by the addition of an anionic detergent, SDS (*37*). The stability of this intermediate at pH 5 was higher than that at a neutral pH. This observation is thus similar to the characteristics of I_{450} of NpHR observed in the present study. In a previous study, it was concluded that this I_{440} of bR would be expected to exhibit a loosely folded protein structure. The formation rate constant and the wavelength at the isosbestic point are both similar to those of NpHR. Although the types of detergents used in these studies differed in terms of being anionic or nonionic, the characteristics of these results nonetheless appeared to be similar. Previously, similar absorption spectra for recombinant wild-type bR in DMPC/CHAPS/SDS-mixed micelles at an acidic pH were observed (*38*). At pH 1.9, the absorption spectra of bR displayed a transition to a species with a λ_{max} at 442 nm in the absence of NaCl. That study concluded that this conversion represents the formation of a free protonated Schiff base (PSB) because of the denaturation of the protein. In contrast, in the presence of 2 M NaCl, a main peak with a λ_{max} at 566 nm was observed at pH 1.9. The results of that experiment suggested that anions can stabilize the PSB of the folded protein by electrostatic interactions. In our study, the visible CD spectra of NpHR−I_{450} did not produce exciton coupling. However, the exciton coupling of NpHR could be slightly recovered, even when the NpHR^{blue} was reconstituted from the acidic I_{450} by neutralization. These results suggest that the I_{450} of the NpHR oligomer has loose packing around the retinal instead of ordered intermolecular interactions, resulting in the formation of a free PSB just like that of bR in the mixed micelles; however, it should be noted that there was a slight λ_{max} difference between the acidic intermediates of bR and NpHR.

It has been reported that bR (*39*−*42*) contains a 9-*cis* retinal under continuous illumination when it is transformed at low pH or in the deionized state. These species exhibit absorption at approximately 430−490 nm as is the case with the bleaching intermediate (I_{450}) of chloride-free NpHR. However, this NpHR intermediate was produced under conditions of nonillumination. As shown in Table 1, it was found that the bleaching intermediate (I_{450}) of chloride-free NpHR contains all-*trans* and 13-*cis* retinals. In addition, a comparison of the reference (*31*) in terms of the HPLC elution pattern of retinaloxime isomers (all-*trans*-, 7-*cis*-, 9-*cis*-, 11-*cis*-, and 13-*cis*-retinals *syn*- and *anti*-oximes) with that of the bleached NpHR in the dark concluded that the bleaching intermediate (I_{450}) of chloride-free NpHR did not contain a 9-*cis* retinal. Investigation of whether NpHR−I_{450} exhibits photoactivity is in progress.

In contrast, the process of the retinal binding of bacterio-opsin (bO), which was reconstituted in the model lipid system with an all-*trans* retinal, has been investigated under dark conditions. bR was reconstituted with bO and the all-*trans* retinal by way of the structural intermediates with λ_{max} values of 380 and 440 nm (*22*, *42*, *43*). These intermediates that occur during the retinal-binding process are apparently similar to those observed in our study. However, the previous study concluded that the retinal-binding intermediate (I_{440}) was constituted with the noncovalently bound retinal, because the bR mutant with a substitution for Lys-216 at the retinal-binding site had a similar absorption maximum at 440 nm (*22*). In our study, it was found that the bleaching intermediate of NpHR−I_{450} has a covalently bound retinal, as identified by the HPLC analysis of retinaloximes (Table 1). In addition, NpHR−I_{450} at a low pH reverted to NpHR^{blue} (600 nm species) and rapidly exhibited a visible CD band with exciton coupling by neutralization, as mentioned above. Thus, our

results support the formation of free PSB, even in the NpHR−I_{450} intermediate. Although the I_{450} intermediate of NpHR accumulated because of the addition of OG, the bleaching process that led to the formation of I_{380} from I_{450} strongly inhibited at an acidic pH. On the other hand, at pH 1.5, the absorbance of the chloride-free NpHR without OG (542 nm) was stable, and this pigment gradually red-shifted by addition of chloride (the opposite spectral shift of NpHR at a neutral pH) such as a property of HsHR. There are only two acidic amino acid residues (Asp156 and Asp252) close to the retinal chromophore of NpHR. It is likely that the PSB in the NpHR is highly protected by the local structure that includes these two acidic residues. Future studies will still be needed to clarify the roles played by these residues and to elucidate the effects of the assembly of NpHR on its stability and function.

ACKNOWLEDGMENT

The authors are very grateful to Dr. Kazumi Shimono (Graduate School of Pharmaceutical Sciences, Hokkaido University) and Prof. Katsutoshi Nitta (Graduate School of Science, Hokkaido University) for invaluable discussions and advice.

REFERENCES

1. Spudich, J. L., Yang, C. S., Jung, K. H., and Spudich, E. N. (2000) Retinylidene proteins: Structures and functions from archaea to humans, *Annu. Rev. Cell Dev. Biol. 16*, 365−392.
2. Booth, P. J., Templer, R. H., Curran, A. R., and Allen, S. J. (2001) Can we identify the forces that drive the folding of integral membrane proteins? *Biochem. Soc. Trans. 29*, 408−413.
3. Váró, G. (2000) Analogies between halorhodopsin and bacteriorhodopsin, *Biophys. Biochem. Acta 1460*, 220−229.
4. Lanyi, J. K. (1990) Halorhodopsin, a light-driven electrogenic chloride-transport system, *Physiol. Rev. 70*, 319−330.
5. Matsuno-Yagi, A., and Mukohata, Y. (1980) ATP synthesis linked to light-dependent proton uptake in a rad mutant strain of *Halobacterium* lacking bacteriorhodopsin, *Arch. Biochem. Biophys. 199*, 297−303.
6. Váró, G., Brown, L. S., Sasaki, H., Kandori, H., Maeda, A., Needleman, R., and Lanyi, J. K. (1995) Light-driven chloride ion transport by halorhodopsin from *Natronobacterium pharaonis*. 1. The photochemical cycle, *Biochemistry 34*, 14490−14499.
7. Váró, G., Needleman, R., and Lanyi, J. K. (1995) Light-driven chloride ion transport by halorhodopsin from *Natronobacterium pharaonis*. 2. Chloride release and uptake, protein conformation change, and thermodynamics, *Biochemistry 34*, 14500−14507.
8. Otomo, J., Tomioka, H., and Sasabe, H. (1992) Properties and the primary structure of a new halorhodopsin from halobacterial strain mex, *Biochim. Biophys. Acta 1112*, 7−13.
9. Soppa, J., Duschl, J., and Oesterhelt, D. (1993) Bacterioopsin, haloopsin, and sensory opsin I of the halobacterial isolate *Halobacterium* sp. strain SG1: Three new members of a growing family, *J. Bacteriol. 175*, 2720−2726.
10. Ihara, K., Umemura, T., Katagiri, I., Kitajima-Ihara, T., Sugiyama, Y., Kimura, Y., and Mukohata, Y. (1999) Evolution of the archaeal rhodopsins: Evolution rate changes by gene duplication and functional differentiation, *J. Mol. Biol. 285*, 163−174.
11. Kolbe, M., Besir, H., Essen, L. O., and Oesterhelt, D. (2000) Structure of the light-driven chloride pump halorhodopsin at 1.8 Å resolution, *Science 288*, 1390−1396.
12. Duschl, A., Lanyi, J. K., and Zimányi, L. (1990) Properties and photochemistry of a halorhodopsin from the haloalkalophile, *Natronobacterium pharaonis*, *J. Biol. Chem. 265*, 1261−1267.
13. Shimono, K., Iwamoto, M., Sumi, M., and Kamo, N. (1997) Functional expression of pharaonis phoborhodopsin in *Escherichia coli*, *FEBS Lett. 420*, 54−56.
14. Hohenfeld, I. P., Wegener, A. A., and Engelhard, M. (1999) Purification of histidine tagged bacteriorhodopsin, pharaonis halorhodopsin, and pharaonis sensory rhodopsin II functionally expressed in *Escherichia coli*, *FEBS Lett. 442*, 198−202.
15. Sato, M., Kanamori, T., Kamo, N., Demura, M., and Nitta, K. (2002) Stopped-flow analysis on anion binding to blue-form halorhodopsin from *Natronobacterium pharaonis*: Comparison with the anion-uptake process during the photocycle, *Biochemistry 41*, 2452−2458.
16. Sato, M., Kikukawa, T., Araiso, T., Okita, H., Shimono, K., Kamo, N., Demura, M., and Nitta, K. (2003) Ser-130 of *Natronobacterium pharaonis* halorhodopsin is important for the chloride binding, *Biophys. Chem. 104*, 209−216.
17. Sato, M., Kikukawa, T., Araiso, T., Okita, H., Shimono, K., Kamo, N., Demura, M., and Nitta, K. (2003) Roles of Ser130 and Thr126 in chloride binding and photocycle of *pharaonis* halorhodopsin, *J. Biochem. 134*, 151−158.
18. Váró, G., Zimányi, L., Fan, X., Sun, L., Needleman, R., and Lanyi, J. K. (1995) Photocycle of halorhodopsin from *Halobacterium salinarium*, *Biophys. J. 68*, 2062−2072.
19. Sato, M., Kubo, M., Aizawa, T., Kamo, N., Kikukawa, T., Nitta, K., and Demura, M. (2005) Role of putative anion-binding sites in cytoplasmic and extracellular channels of *Natronomonas pharaonis* halorhodopsin, *Biochemistry 44*, 4775−4784.
20. Zimányi, L., and Lanyi, J. K. (1997) Fourier transform Raman study of retinal isomeric composition and equilibration in halorhodopsin, *J. Phys. Chem. B 101*, 1930−1933.
21. Lanyi, J. K. (1997) Mechanism of ion transport across membranes. Bacteriorhodopsin as a prototype for proton pumps, *J. Biol. Chem. 272*, 31209−31212.
22. Lu, H., and Booth, P. J. (2000) The final stages of folding of the membrane protein bacteriorhodopsin occur by kinetically indistinguishable parallel folding paths that are mediated by pH, *J. Mol. Biol. 299*, 233−243.
23. Yokoyama, Y., Sonoyama, M., and Mitaku, S. (2004) Inhomogeneous stability of bacteriorhodopsin in purple membrane against photobleaching at high temperature, *Proteins 54*, 442−454.
24. Mukai, Y., Kamo, N., and Mitaku, S. (1999) Light-induced denaturation of bacteriorhodopsin solubilized by octyl-β-glucoside, *Protein Eng. 12*, 755−759.
25. Sasaki, T., Sonoyama, N., Demura, M., and Mitaku, S. (2005) Photobleaching of bacteriorhodopsin solubilized with Triton X-100, *Photochem. Photobiol.*, in press.
26. Guereca, L., and Bravo, A. (1999) The oligomeric state of *Bacillus thuringiensis* Cry toxins in solution, *Biochim. Biophys. Acta 1429*, 342−350.
27. Osawa, M., Tong, K. I., Lilliehook, C., Wasco, W., Buxbaum, J. D., Cheng, H.-Y. M., Penninger, J. M., Ikura, M., and Ames, J. B. (2001) Calcium-regulated DNA binding and oligomerization of the neuronal calcium-sensing protein, calsenilin/DREAM/KChIP3, *J. Biol. Chem. 276*, 41005−41013.
28. Scharf, B., and Engelhard, M. (1994) Blue halorhodopsin from *Natronobacterium pharaonis*: Wavelength regulation by anions, *Biochemistry 33*, 6387−6393.
29. Henry, E. R., and Hofrichter, J. (1992) Singular value decomposition: Application to analysis of experimental data, *Methods Enzymol. 210*, 129−193.
30. Shimono, K., Ikeura, Y., Sudo, Y., Iwamoto, M., and Kamo, N. (2001) Environment around the chromophore in *pharaonis* phoborhodopsin: Mutation analysis of the retinal binding site, *Biophys. Biochem. Acta 1515*, 92−100.
31. Tsukida, K., Ito, M., Tanaka, T., and Yagi, I. (1985) High-performance liquid chromatographic and spectroscopic characterization of stereoisomeric retinaloximes. Improvements in resolution and implication of the method, *J. Chromatogr. 331*, 265−272.
32. Walter, A., Kuehl, G., Barnes, K., and VanderWaerdt, G. (2000) The vesicle-to-micelle transition of phosphatidylcholine vesicles induced by nonionic detergents: Effects of sodium chloride, sucrose, and urea, *Biochim. Biophys. Acta 1508*, 20−33.
33. Imamoto, Y., Shichida, Y., Hirayama, J., Tomioka, H., Kamo, N., and Yoshizawa, T. (1992) Chromophore configuration of *pharaonis* phoborhodopsin and its isomerization on photon absorption, *Biochemistry 31*, 2523−2528.
34. Oesterhelt, D., and Stoeckenius, W. (1971) Rhodopsin-like protein from the purple membrane of *Halobacterium halobium*, *Nature 233*, 149−152.
35. Zhang, R., and Somasundaran, P. (2004) Abnormal micellar growth in sugar-based and ethoxylated nonionic surfactants and their

mixtures in dilute regimes using analytical ultracentrifugation, *Langmuir 20*, 8552–8558.
36. Duschl, A., McCloskey, M. A., and Lanyi, J. K. (1988) Functional reconstitution of halorhodopsin. Properties of halorhodopsin-containing proteoliposomes, *J. Biol. Chem. 263*, 17016–17022.
37. London, E., and Khorana, H. G. (1982) Denaturation and renaturation of bacteriorhodopsin in detergents and lipid-detergent mixtures, *J. Biol. Chem. 257*, 7003–7011.
38. Marti, T., Rosselet, S. J., Otto, H., Heyn, M. P., and Khorana, H. G. (1991) The retinylidene Schiff base counterion in bacteriorhodopsin, *J. Biol. Chem. 266*, 18674–18683.
39. Fischer, U. C., Towner, P., and Oesterhelt, D. (1981) Light induced isomerisation, at acidic pH, initiates hydrolysis of bacteriorhodopsin to bacterio-opsin and 9-*cis*-retinal, *Photochem. Photobiol. 33*, 529–537.
40. Zimanyi, L., and Lanyi, J. K. (1987) Iso-halorhodopsin: A stable, 9-*cis* retinal containing photoproduct of halorhodopsin, *Biophys. J. 52*, 1007–1013.
41. Pande, C., Callender, R. H., Chang, C. H., and Ebrey, T. G. (1986) Resonance Raman study of the pink membrane photochemically prepared from the deionized blue membrane of *H. halobium*, *Biophys. J. 50*, 545–549.
42. Gaertner, W., Towner, P., Hopf, H., and Oesterhelt, D. (1983) Removal of methyl groups from retinal controls the activity of bacteriorhodopsin, *Biochemistry 22*, 2637–2644.
43. Booth, P. J., and Farooq, A. (1997) Intermediates in the assembly of bacteriorhodopsin investigated by time-resolved absorption spectroscopy, *Eur. J. Biochem. 246*, 674–680.

BI0511235

International Immunology, Vol. 17, No. 11, pp. 1463–1471
doi:10.1093/intimm/dxh324
© The Japanese Society for Immunology. 2005. All rights reserved.
For permissions, please e-mail: journals.permissions@oupjournals.org

Active repression of IFN regulatory factor-1-mediated transactivation by IFN regulatory factor-4

Kayo Yoshida[1], **Kazuo Yamamoto**[1], **Tomoko Kohno**[1], **Noriko Hironaka**[1], **Kiyoshi Yasui**[1], **Chojiro Kojima**[2], **Hiroshi Mukae**[3], **Jun-ichi Kadota**[4], **Shoichi Suzuki**[5], **Kiri Honma**[6], **Shigeru Kohno**[3] and **Toshifumi Matsuyama**[1]

[1]Division of Cytokine Signaling, Department of Molecular Microbiology and Immunology, Nagasaki University Graduate School of Biomedical Sciences, 1-12-4 Sakamoto, Nagasaki 852-8523, Japan
[2]Laboratory of Biophysics, Department of Molecular Biology, Nara Institute of Science and Technology, Ikoma, Nara 630-0101, Japan
[3]Second Department of Internal Medicine, Nagasaki University School of Medicine, Nagasaki 852-8501, Japan
[4]Second Department of Internal Medicine, Oita University Faculty of Medicine, Oita-gun, Oita 879-5593, Japan
[5]Department of Host-Defense Biochemistry, Institute of Tropical Medicine, Nagasaki University, Nagasaki 852-8523, Japan
[6]Division of Immunology, Department of Molecular Medicine, Nagasaki University Graduate School of Biomedical Sciences, Nagasaki 852-8523, Japan

Keywords: gene regulation, IRF-1, IRF-4, lymphocytes, transcription factors

Abstract

IFN regulatory factor-4 (IRF-4) is a transcription factor that is involved in the development and the functions of lymphocytes, macrophages and dendritic cells. Despite their critical roles in immune system regulation, the target genes controlled by IRF-4 are poorly understood. In this study, we determined the consensus DNA-binding sequences preferred for IRF-4 by *in vitro* binding site selections. IRF-4 preferentially bound to the sequences containing tandem repeats of 5′-GAAA-3′, flanked by CpC, in most cases. IRF-4 repressed the promoter bearing tandem copies of the selected binding sequence, while IRF-1 activated the same constructs. Interestingly, the IRF-1-dependent transactivation is inhibited in the presence of IRF-4, but not IRF-2. A series of deletion mutants of IRF-4 revealed that its DNA-binding domain was necessary and sufficient to antagonize the IRF-1-dependent transactivation. This dominant negative action of IRF-4 over IRF-1 was also observed in a natural promoter context, such as the TRAIL gene. These results indicate that IRF-4 acts as a natural antagonist against IRF-1 in immune cells.

Introduction

IFN regulatory factors (IRFs) constitute a family of transcription factors that mediate IFN signaling, confer an anti-viral state and modulate the immune system. Ten cellular members and several virus-encoded IRF genes have been identified to date. Some IRFs are immune cell specific, while others are ubiquitously expressed (1–3). All IRFs share significant homology within the amino-terminal DNA-binding domain (DBD), which is characterized by a winged helix-turn-helix motif with five tryptophan repeats. Through this domain, activation by IFN-α/β typically induces IRF family members to bind to the IFN-stimulated response elements (ISRE) found within IFN-responsive genes (4). Some IRF proteins also contain the IRF association domain (IAD) within the carboxyl-terminus, through which protein–protein interactions with IRFs or non-IRF proteins are believed to occur. This domain is common to IRF-3, IRF-4, IRF-5, interferon consensus sequence binding protein/IRF-8 and ISGF3γ/IRF-9, but not to IRF-1, IRF-2, IRF-6 or IRF-7.

IRF-4 is a member of the IRF family, and its expression is restricted to immune cells, such as lymphocyte, macrophage and dendritic cells (5–9). It is not induced by IFNs, but rather by antigen-receptor-mediated stimuli, such as plant lectins, CD3 or IgM cross-linking (6). Consistent with its highly limited expression, the deficiency in IRF-4 was manifested in very specific manners in the immune system (10). As for B cell function, the serum immunoglobulin levels were dramatically reduced and the antibody responses were absent. IRF-4-deficient T lymphocytes showed a reduced proliferative response and lower cytokine production, and lacked cytotoxic and anti-tumor responses (10). IRF-4 was essential for the T_h2

Correspondence to: T. Matsuyama; E-mail: tosim@net.nagasaki-u.ac.jp
Transmitting editor: H. Karasuyama

Received 17 December 2004, *accepted* 23 August 2005
Advance Access publication 19 September 2005

response (11–13). Interestingly, this response seems to be attributable not only to IRF-4-expressing T_h2 cells but also to dendritic cells, as we recently discovered the importance of IRF-4 in the development of $CD11b^{high}$ $CD8\alpha^-$ dendritic cells, which are important to polarize T_h0 cells to T_h2 (14). In contrast to the wealth of information about the physiological significance mentioned above, the downstream molecules of IRF-4 have remained essentially uncharacterized.

IRF-4 was initially identified as a transcriptional activator. This function was linked to a physical interaction with the hematopoietic cell-specific transactivator, PU.1, on a composite Ets/ISRE element within the Igλ light chain enhancer in B cells (5). IRF-4 also associates with E47, Stat6, Bcl-6 and NFATc2 to synergistically activate particular genes (11, 15, 16). On the other hand, IRF-4 was reported to function as a transcriptional repressor when bound to the ISRE DNA motifs of some genes (7). Thus, IRF-4 may serve as either an activator or a repressor, depending on the context of the DNA-binding sequences and/or the protein-interaction partners. To clarify the former, we tried to determine the optimal DNA sequence recognized by IRF-4 in the absence of protein-interaction partners. Here we report that the selected binding sequence was a defined derivative of the consensus ISRE. We describe our functional characterizations of the selected binding sequence both *in vitro* and *in vivo*.

Methods

Cell culture

HeLa cells were grown in DMEM supplemented with 10% FCS and 100 U ml^{-1} penicillin–streptomycin in a 37°C incubator with 5% CO_2 and 100% humidity. DMEM was purchased from Sigma (St Louis, MO, USA). FCS was purchased from Life Technologies (Rockville, MD, USA). 293 T cells were grown in αMEM supplemented with 10% FCS and 100 U ml^{-1} penicillin–streptomycin in a 37°C incubator with 5% CO_2 and 100% humidity. αMEM was purchased from GIBCO BRL (Gaithersburg, MD, USA).

Selected and amplified binding sites determination

Selected and amplified binding site (SAAB) selection was done essentially as described by Blackwell and Weintraub (17), using affinity chromatography. The 'random' oligonucleotide contained 20 random nucleotides flanked by the known sequences 'b' and 'a', which could be recognized by the PCR primers 'b' (5′-AGACGGATCCATTGCA-3′) and 'a' (5′-TCCGAATTCCTACAG-3′), respectively [sequences from Blackwell and Weintraub (17)]. Double-stranded random oligonucleotides were generated by annealing 1.5 μg of the single-stranded random oligonucleotide with 0.7 μg of the PCR primer 'a', followed by filling-in with Klenow DNA polymerase. The double-stranded oligonucleotides (0.4 μg) were incubated with the glutathione-*S*-transferase (GST)–IRF-4 fusion protein (400 ng) attached to glutathione-Sepharose beads in binding buffer [10 mM HEPES-KOH (pH 7.9), 0.2 M NaCl, 0.5 mM EDTA, 0.5 mM dithiothreitol (DTT) and 0.5 mM phenylmethylsulfonylfluoride (PMSF)] with 200 μg ml^{-1} poly(dG):poly(dC) at room temperature for 30 min. The beads were recovered by brief centrifugation, washed twice with binding buffer, suspended in 30 μl of H_2O and incubated at 95°C for 5 min to release the oligonucleotides bound to the GST–IRF-4 affinity beads. A 10-μl aliquot was then used for PCR amplification in a 25-μl reaction for 30 cycles of 94°C (30 s), 38°C (30 s) and 72°C (30 s). For subsequent rounds, a 10-μl aliquot of the PCR was incubated with 40 ng of protein. After five rounds of selection, the recovered oligonucleotides were digested with *Bam*HI and *Eco*RI, cloned into pBluescript KS(+) and subjected to sequence analysis.

Plasmid constructions

To construct an expression plasmid for the GST–IRF-4 fusion protein, the human IFN regulatory factor-4 (hIRF-4) cDNA was inserted into the pGEX vector (Amersham Pharmacia Biotech, Uppsala, Sweden), via the *Bam*HI and *Eco*RI sites. Flag-tagged hIRF-4 cDNA was excised from the plasmid pBluescript Flag–hIRF-4 by *Hin*dIII and *Xba*I digestions and then ligated into the corresponding sites of the pcDNA3 vector (Invitrogen, San Diego, CA, USA). Detailed information about the construction of the plasmid pBluescript Flag–hIRF-4 will be provided upon request.

To prepare the hIRF-4 carboxyl-terminal deletion protein 1–129, pcDNA3 Flag–hIRF-4 was digested with *Eco*81I and *Xba*I, blunt ended by Klenow polymerase and then self-ligated. To prepare the hIRF-4 carboxyl-terminal deletion proteins 1–200 and 1–336, pcDNA3 Flag–hIRF-4 was digested with *Sac*II or *Apa*I, blunt ended by T4 DNA polymerase and then self-ligated. To prepare the hIRF-4 carboxyl-terminal deletion protein 1–432, pBluescript Flag–hIRF-4 was digested with *Spe*I and *Bgl*II, blunt ended by Klenow polymerase and self-ligated to yield the plasmid pBluescript Flag–hIRF-4 1–432. This plasmid was digested with *Hin*dIII and *Xba*I, and the DNA fragment containing the Flag–hIRF-4 1–432 sequence was recovered and ligated into the corresponding sites of pcDNA3. The *Nde*I–*Pvu*II fragment of pBluescript Flag–hIRF-4 was replaced by a linker DNA (5′-CGTTAACG-3′). Then, the *Hin*dIII–*Xba*I fragment containing Flag–hIRF-4 116–450 was recovered and ligated into the corresponding sites of pcDNA3.

Human IRF-1 and IRF-2 were amplified by PCR and inserted into the *Nde*I and *Not*I sites, respectively, of the plasmid pBluescript Flag–PAF49. The resultant plasmids, pBluescript Flag–hIRF-1 and pBluescript Flag–hIRF-2, were digested with *Bam*HI and *Not*I, and then the Flag–hIRF-1 and Flag–hIRF-2 fragments were ligated into the corresponding sites of pcDNA3, respectively. For the construction of reporter plasmids containing one, two or four copies of the selected binding site, the double-stranded oligonucleotides (5′-GCCCCGAAACCGAAACCATGC-3′) were tandemly ligated and cloned into the *Sma*I site of the pGL2-Promoter vector (Promega, Madison, WI, USA). The region of DNA containing the DBD of IRF-4 was obtained by PCR with the following primer set: 5′-GGAATCCATATGGGCAACGGGAAGCTCCGCCAGTGG-3′/5′-CCGCTCGAGTCCTTTTTTGGCTCCCTCAGGAAC-3′. The PCR product was digested with *Nde*I and *Xho*I, and inserted into the corresponding sites of the expression vector pET21a (+).

The human TRAIL promoter constructs were kindly provided by B. Mark Evers, University of Texas Medical Branch (18). Point mutations were introduced in the putative ISRE sites on

the TRAIL promoter by the Quick Change Site-Directed Mutagenesis Kit, according to the manufacturer's instructions (Stratagene, La Jolla, CA, USA).

The $SAAB_{DCIR}$ luciferase vector was constructed in the pGL3 promoter vector with the concatemer consisting of four tandem repeats of a candidate SAAB motif, ACACGAAACC-GAAACCT, found in human dendritic cell immunoreceptor (DCIR) gene promoter.

Protein preparation

Escherichia coli TG1 cells harboring pGEX hIRF-4 were grown in LB medium at 30°C to an optical density of 0.6 at 600 nm, and then isopropyl-β-D-thiogalactopyranoside was added to a 2 mM final concentration and the culture was further incubated for 3 h. Cells were re-suspended in PBS supplemented with 0.5 mM PMSF, and then lysed by sonication. Cellular debris was removed by ultracentrifugation. The supernatant was used for the SAAB assay. For EMSA, *E. coli* BL21 (DE3) cells harboring the plasmid pET-hIRF4DBD were grown, and the lysate was prepared as described above. The lysate was applied to a HisTrap column (Amersham Pharmacia Biotech), and then the column was washed with PBS supplemented with 10 mM imidazole. Bound proteins were eluted by PBS supplemented with 200 mM imidazole. The eluted proteins were desalted by passage through a PD-10 column (Amersham Pharmacia Biotech) in the presence of an assay buffer containing 20 mM HEPES-KOH (pH 7.9), 100 mM KCl, 0.2 mM EDTA, 1 mM DTT and 20% glycerol. Protein concentrations were determined by the standard Bradford assay, and then the eluted proteins were aliquoted and stored at −80°C.

Reverse transcription–PCR

Splenic T cells were enriched from a spleen cell suspension by density-gradient centrifugation on Lympholyte-M (Cedarlane Laboratories, Ontario, Canada), and then were negatively selected with a Pan T Cell Isolation Kit (Miltenyi Biotec, Germany). Total RNA was isolated from splenic T cells of wild-type, IRF-$1^{-/-}$, IRF-$4^{-/-}$ and IRF-$1^{-/-}$,IRF-$4^{-/-}$ mice, which were either unstimulated or stimulated by Con A for 6, 12 and 24 h, using the ISOGEN reagent according to the manufacturer's protocol (Nippon Gene, Tokyo, Japan). The first-strand cDNA was synthesized using the ProSTAR first-strand RT–PCR kit (Stratagene) with oligo(dT) primers. One microliter of the first-strand cDNA reaction was used in a 20-μl PCR amplification with the specific primers for murine DCIR (5′-GTGAT-CCAGAGCCAGGAAGA-3′/5′-TCATCTGAGTGCCAGGATGT-3′) and β-actin (5′-TGGAATCCTGTGGCATCCATGAAAC-3′/ 5′-TAAAACGCAGCTCAGTAACAGTCCG-3′), respectively. Cycling conditions were as follows: denaturing at 94°C for 60 s, annealing at 56°C for 60 s for DCIR and at 60°C for 60 s for β-actin and extension at 72°C for 60 s.

Reporter assays

HeLa or 293T cells (1.5×10^5) were seeded into six-well plates and transfected with 1 μg reporter plasmid and 1 ng pRLβ-actin as an internal control (19), together with up to 1 μg of pcDNA3, pcDNA3Flag-hIRF1 or pcDNA3Flag-hIRF4. Twenty-four hours after transfection, extracts were prepared from the transfected cells and the luciferase activity was determined using the Dual Luciferase Assay kit, according to the manufacturer's protocol (Promega). The luciferase activity was normalized with the *Renilla* luciferase activity from the internal control, and is represented as the relative luciferase activity.

PBMCs were prepared from blood according to the standard Ficol Paque protocol, and were subjected to gene transfer using the Nucleofector equipment, according to the manufacturer's recommendations (Amaxa Biosystems, Allemagne, Germany). Typically, 2×10^6 PBMCs were used for the Nucleofection with 1 μg reporter plasmid and 1 ng pRLβ-actin as an internal control, together with 1 μg of pcDNA3, pcDNA3Flag-hIRF1 or pcDNA3Flag-hIRF4, to keep the total amount of plasmid at 3 μg. Cells were cultured in DMEM containing 10% fetal bovine serum with antibiotics for 24 h after Nucleofection, and then were harvested for the luciferase assay.

Nuclear extract preparation

Nuclear extracts were prepared according to the method of Schreiber *et al.* (20). Briefly, 5×10^5 cells were treated with 250 U ml^{-1} IFN-γ. After 12 h, the cells were washed with ice-cold PBS, suspended in 200 μl of buffer A [10 mM HEPES-KOH (pH 7.9), 10 mM KCl, 0.1 mM EDTA, 1 mM DTT and 0.5 mM PMSF] and incubated on ice for 15 min. The cells were then lysed in the presence of 0.6% Nonidet P-40 by vortexing for 10 s. The nuclei were collected by centrifugation for 15 s and were suspended in 50 μl of buffer C [20 mM HEPES-KOH (pH 7.9), 400 mM NaCl, 1 mM EDTA, 1 mM DTT and 1 mM PMSF] at 4°C for 15 min. The nuclear extracts were recovered after centrifugation at 15 000 r.p.m. for 5 min and were stored at −80°C.

EMSA

The oligonucleotides used in this study had the following sequences: SAAB1, 5′-GCCCCGAAACCGAAACCATGC-3′, and GBP-ISRE, 5′-GAATATGAAACTGAAAGTACTT-3′. The double-stranded DNAs were labeled by a filling-in reaction at the 5′-G overhangs with Klenow enzyme and [α-^{32}P]dCTP. Binding reactions were conducted with 2 μl of nuclear extracts in a 10-μl reaction containing 10 mM HEPES-KOH (pH 7.9), 50 mM NaCl, 0.1 mM EDTA, 0.5 mM DTT, 0.5 mM PMSF, 10% glycerol and 100 μg ml^{-1} poly (dG):poly (dC). After a 20-min pre-incubation on ice, the end-labeled probe (5000 c.p.m.) was added, and the reaction was incubated at 25°C for 30 min. In some cases the reactions were further incubated with anti-IRF-1 antibody (C-20; Santa Cruz Biotechnology, Santa Cruz, CA, USA) or anti-His antibody (His-probe; Santa Cruz Biotechnology) at 25°C for 30 min. The binding reactions were mixed with 1 μl of loading buffer (0.1% bromophenol blue, in the same buffer as that used for the binding reactions) and then electrophoresed on a non-denaturing 5% polyacrylamide gel with 0.5× TBE at 25°C. The gels were dried and analyzed using an image analyzer (BAS5000, Fuji).

Results

Determination of the optimal DNA-binding sequence of IRF-4

To determine the optimal DNA-binding sequence of IRF-4, the SAAB selection assay was performed with recombinant

GST–IRF-4 fusion protein (17). Oligonucleotides containing 20 random nucleotides, flanked by known sequences that could be recognized by PCR primers, were annealed with one of the PCR primers, and then converted to the double-stranded form by the Klenow enzyme. The double-stranded oligonucleotides were incubated with GST–IRF-4 attached to glutathione-Sepharose beads. The beads were collected, and the bound oligonucleotides were eluted and amplified by PCR. For subsequent rounds, the PCR products were incubated with GST–IRF-4 and the bound oligonucleotides were further selected. Repeating the binding-selection cycle several times should concentrate the oligonucleotides that have higher binding affinity to IRF-4. The sequences of the oligonucleotides selected after five sequential SAAB rounds are shown in Fig. 1. In general, all the selected oligonucleotides contained one or two copies of the ISRE core sequence, 5′-GAAA-3′. It is interesting to note that CpC dinucleotides are preferred for the sequences flanking the core sequence.

To examine whether IRF-4 can bind to the selected sequence, we performed an EMSA. As shown in Fig. 2, IRF-4 can bind to one of the representative selected sequences (SAAB1, 5′-GCCCCGAAACCGAAACCATGC-3′). The DNA–protein complex was challenged by a competition with excess amounts of unlabeled oligonucleotides. The SAAB1 sequence competed well with the probe DNA (lanes 3–5), similar to the ISRE of the guanine-binding protein gene (GBP), a well-known sequence used as the target for IRF family proteins (7) (lanes 6–8). These results clearly demonstrate that the selected sequence actually binds to IRF-4 with sufficiently high affinity.

Transcriptional repression by IRF-4

To examine whether the selected sequences function *in vivo*, we constructed luciferase reporters containing one, two or four copies of SAAB1, and transfected them into HeLa cells (Fig. 3). The promoter activity was increased, depending on the SAAB1 copy number (Fig. 3A), probably due to the activities of the intrinsic IRFs. Actually, IRF-1 could activate the reporter activity, in an SAAB1 sequence-dependent manner (Fig. 3B). In contrast, IRF-4 actively repressed the spontaneous activation of the SAAB1-Luc reporter gene (Fig. 3A). We also examined the effect of IRF-2, but it showed only a marginal repression of the SAAB1-Luc reporter gene (Fig. 3B). Next, we compared the effect of IRF-2 or IRF-4 on IRF-1 transactivation (Fig. 3C). IRF-2 is known to repress the IRF-1-mediated induction of several genes, such as IFN-β and major histocompatibility complex class I genes (1–3, 7). However, IRF-2 did not repress the IRF-1-mediated transactivation of the SAAB1-containing promoter. In contrast, IRF-4 reduced the IRF-1-mediated activation of the promoter almost to the basal level, even with only a small amount of the IRF-4 expression vector DNA. These results suggest that the selected sequence can serve as the target for the activation by IRF-1 and for the repression by IRF-4.

The DBD of IRF-4 is necessary and sufficient for the antagonistic effect against IRF-1

To examine the mechanism by which IRF-4 represses IRF-1-mediated transactivation, we constructed a series of deletion mutants of IRF-4 (Fig. 4). Structure–function analyses revealed

CATGAG**GAAACCGAAACCA**C
CC**CAC**A**GAAACCGAAACCA**G
CC**CA**G**CGAAACCGAAACCA**TG
C**CCCCGAAACCGAAACCA**TG
TA**CCCGAAACCGAAACCA**TG
C**CC**A**CGAAACCGAAAC**GACG
CCCCGAAACCGAAACTGGTG
CACCGAAACCGAATCCATGG
CA**CCCGAAACCGAATCCA**GG
C**CCCCGAAACCGAATCCA**GG
C**CACCGAAACCGAATCC**GTG
CACCGAAACCGAATCCAGGG
CACCGAAACCGAATCCATGG
CACA**ACCGAAACCGA**T**ACCA**CG
CA**CACCGAAA**G**CGA**T**ACCA**G
CACCGAAAG**CGAATCCA**GGG
CCCCGAAAG**CGAATCCA**TGG
CACCGAAAG**CGAATCCA**GGG
CCCA**GAAA**T**CGAAACCA**TAG

5′-C$^{A}/_{C}$CCGAAACCGAA$^{A}/_{T}$CCA-3′

Fig. 1. SAAB determination for IRF-4. The sequences of 19 cloned IRF-4-binding sites selected by five rounds of selection are shown. The DNA sequences were aligned to develop a consensus sequence. Homologous (>80%) sequences are in boldface. The consensus sequence is also shown.

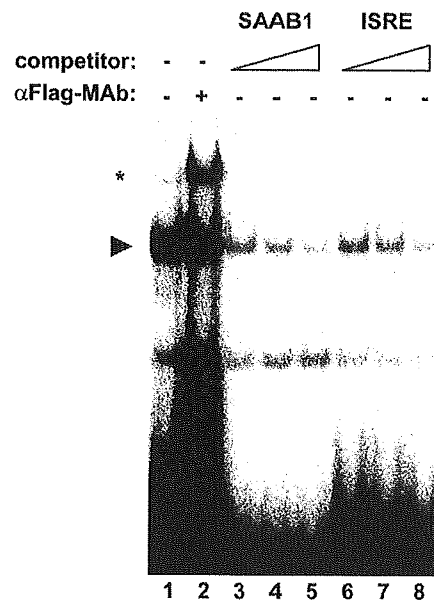

Fig. 2. Binding capacity of the selected sequence to IRF-4. Nuclear extracts from HeLa cells transfected with the Flag-tagged hIRF-4 expression plasmid were incubated with the radiolabeled IRF-4-binding consensus sequence (SAAB1), in the absence (lanes 1–2) or presence of a 5-, 10- or 20-fold excess amount of unlabeled SAAB1 (lanes 3–5) or ISRE of the GBP gene (lanes 6–8) as competitor DNAs. An anti-Flag mAb was also included in the binding reaction to verify the presence of the Flag-tagged IRF-4 protein (lane 2). The arrowhead indicates the IRF-4–DNA complex, and the asterisk shows a supershift signal that is formed by the binding of the antibody to the IRF-4–DNA complex.

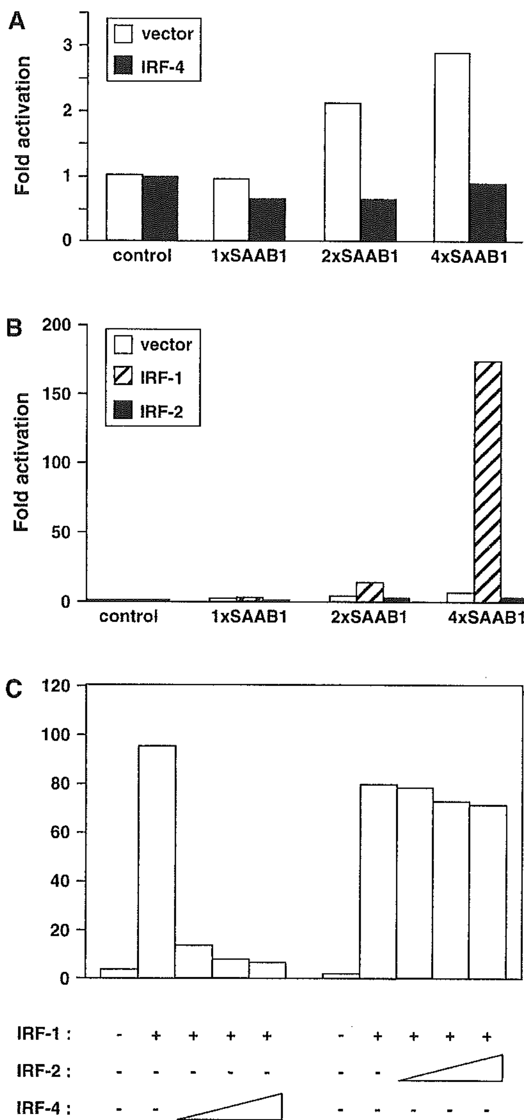

Fig. 3. The selected binding sites serve as the target for IRF-4 and IRF-1. (A) HeLa cells were transfected with reporter constructs containing one, two or four copies of SAAB1, and either the IRF-4 expression plasmid (solid bars) or the empty vector (open bars). Luciferase activity was assayed at 24 h post-transfection. The firefly luciferase activity was normalized to the *Renilla* luciferase activity from the internal control plasmid, which was transfected simultaneously. Fold activations are indicated as relative values to the normalized luciferase activity of the parental reporter plasmid pGL2-Promoter. Each column represents the mean from three independent experiments. (B) Luciferase assays were performed as described with the reporter constructs containing one, two or four copies of SAAB1, and the expression plasmid of IRF-1 (hatched bars) or IRF-2 (solid bars), or empty vector (open bars). (C) IRF-4 antagonizes IRF-1-dependent transactivation. HeLa cells were transfected with the reporter construct containing four copies of SAAB1 (4 × SAAB1), with (denoted by '+') or without (denoted by '–') 0.5 μg of the expression plasmid for IRF-1, together with increasing amounts (0.125, 0.25 and 0.5 μg) of either IRF-4 or IRF-2 expression plasmid. The total amount of DNA was held constant by including an empty vector in the transfection mixtures. Luciferase activities are presented as fold activation, as described above.

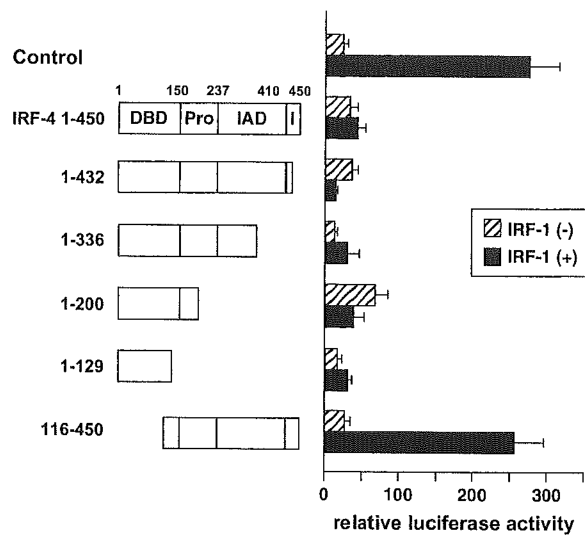

Fig. 4. The DBD of IRF-4 is necessary and sufficient for the repression of IRF-1-mediated transactivation. The deletion mutants of IRF-4 are schematically represented on the left. The functional domains of IRF-4 are defined as follows: DBD, DNA-binding domain (aa 1–150); Pro, a proline-rich region (aa 151–237); IAD, an IRF association domain (aa 238–410); I, a C-terminal autoinhibition domain (aa 411–450). HeLa cells were transfected with the 4 × SAAB1 reporter construct, with (represented by solid bars) or without (represented by hatched bars) 0.5 μg of the IRF-1 expression plasmid, together with 0.5 μg of each IRF-4 deletion construct or an empty vector. The luciferase assay was performed as described in Fig. 3.

that IRF-4 contains the N-terminal DBD [located between amino acids (aa) 1 and 150], the proline-rich region (aa 150–237), the IAD (aa 237–410) and the C-terminal autoinhibition domain (aa 410–450) (1–3). Deletion of up to 321 aa from the C-terminus of IRF-4 had no effect on the repression activity for the IRF-1-mediated transactivation. In contrast, the removal of 115 residues from the N-terminus caused a complete loss of the repression activity. These results clearly indicate that the IRF-4 DBD is necessary and sufficient for the antagonizing effect against IRF-1-mediated transactivation.

IRF-1 transactivates the TRAIL promoter

We next examined the effects of IRF-4 and IRF-1 on the SAAB sequences in a natural promoter context *in vivo*. For this purpose, we searched the human genome database for sequences similar to the selected sequences in the known gene promoter, and found that the human TRAIL gene promoter contains two sequences, one (–129 to –140) that exactly matches and another (+4 to –8) that is highly homologous to one of the selected sequences (Fig. 5A). The luciferase reporter construct containing a 1.6-kb fragment of the human TRAIL promoter region (–1523) was dramatically activated by IRF-1 (Fig. 5B). Deletion of the 5′-upstream region up to –165 had no effect on the response to IRF-1, indicating that this region contains the elements that can confer the IRF-1 responsiveness to the promoter. We then mutated the two SAAB-like sequences found in this region, individually or simultaneously. Mutations in the distal site

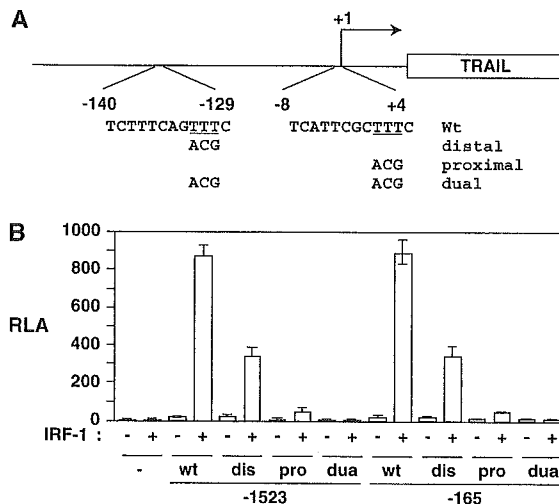

Fig. 5. The SAAB-like sequences in the human TRAIL promoter respond to IRF-1. (A) Schematic representation of luciferase reporter constructs containing the human TRAIL promoter. The SAAB-like sequences and the corresponding mutations are indicated. (B) 293T cells were co-transfected with the TRAIL promoter–luciferase reporter plasmid with an internal control luciferase vector, together with pcDNA3Flag–hIRF-1 or an empty pcDNA3 vector. After 24 h, the luciferase activity was analyzed. The results shown are the averages of three independent experiments with standard deviation.

(−140 TCTTTCAGACGC −129) resulted in more than a 50% reduction in the transactivation by IRF-1. When we introduced mutations in the proximal site (−8 TCATTCGCACGC +4), the response of the promoter to IRF-1 was reduced to one-tenth of that of the wild-type promoter. It should be noted that this region does not include the consensus initiator sequence, which functions as a core promoter element for some particular genes (22), suggesting that the mutated sequence did not violate the basal promoter activity. When the distal and proximal sites were mutated simultaneously, the promoter completely lost the ability to respond to IRF-1, indicating a synergistic activity of these sites. These results clearly demonstrate that the SAAB-like sequences found in the human TRAIL promoter actually serve as the target of IRF-1, and suggest that TRAIL gene expression is regulated by IRF family transcription factors.

Dominant action of IRF-4 over IRF-1 on human TRAIL gene expression

Next, we examined the effect of IRF-4 on the transactivation of the human TRAIL promoter by IRF-1. To do this, the TRAIL–luciferase construct was introduced into 293T, together with the expression vectors of IRF-1 and/or IRF-4. As shown in Fig. 6A, IRF-1 activated the TRAIL promoter, while IRF-4 alone showed marginal transactivation of the promoter. Co-transfection of IRF-4 and IRF-1 reduced the promoter activity significantly. As expected, IRF-2 failed to reduce the promoter activity of the TRAIL gene activated by IRF-1 (Fig. 6B). We also examined whether a similar finding would be obtained with PBMC, in the natural context. To do this, the TRAIL–luciferase construct was introduced into PBMCs, together with the

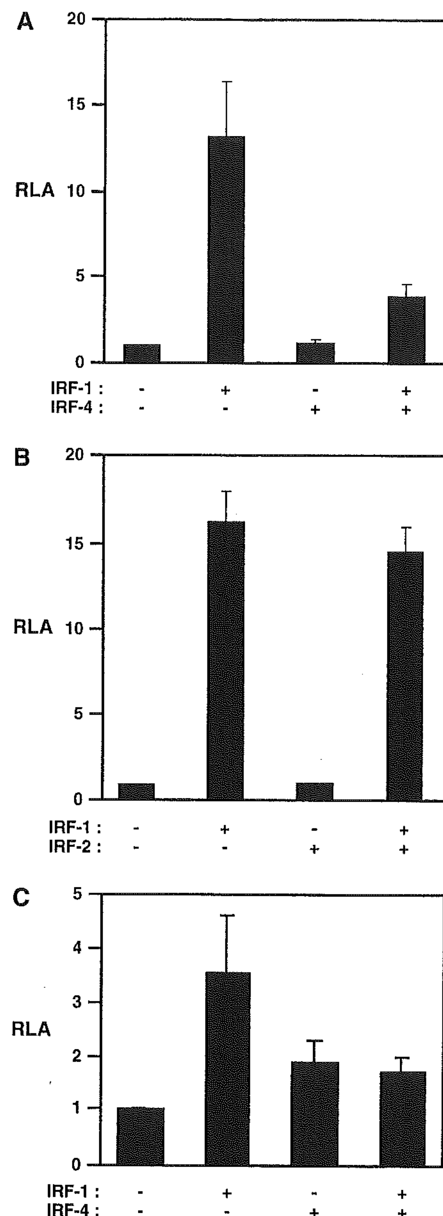

Fig. 6. The repression of IRF-1-mediated transactivation by IRF-4 in the human TRAIL promoter. (A) 293T cells containing the human TRAIL–luciferase constructs were co-transfected with the IRF-1 and/or IRF-4 expression vector. After a 24-h incubation, the luciferase activity was analyzed. The results shown are the averages of three independent experiments with standard deviation. (B) Experiments were done as in (A), with the exception that IRF-2, but not IRF-4, expression vector was used. (C) Experiments were done as in (A), with the exception that PBMCs were used.

expression vectors of IRF-1 and/or IRF-4. As shown in Fig. 6C, IRF-1 activated the TRAIL promoter in PBMCs, while IRF-4 alone showed marginal transactivation of the promoter. Co-transfection of IRF-4 and IRF-1 reduced the promoter activity to the same extent, as observed for IRF-4 only. These results

indicate that IRF-4 works as a dominant negative effector to IRF-1 in the natural promoter context *in vivo*.

Expression of the DCIR gene is regulated by IRF-1 and IRF-4

We also searched the mouse genome database, and found that the 3′-UTR of the murine DCIR gene contains a sequence highly homologous to the selected consensus sequence (5′-ACACGAAACCGAAACCT-3′). We thus analyzed DCIR mRNA induction following Con A stimulation in mouse splenic T cells. As shown in Fig. 7A, real-time reverse transcription–PCR revealed that the DCIR mRNA was induced by the Con A treatment in the wild-type splenic T cells. The Con A-dependent induction of the DCIR mRNA was augmented in the IRF-4-deficient cells. In contrast, the DCIR mRNA was not induced in IRF-1-deficient cells. Consistently, we demonstrated that IRF-1 transactivates the SAAB-like motif of DCIR, and this was inhibited by the presence of IRF-4 (Fig. 7B). These results suggest that the expression of DCIR strictly depends on the concerted actions of IRF-1 and IRF-4.

Discussion

In the present study, we tried to establish the range of IRF-4 activity by determining the DNA sequences recognized by IRF-4. The *in vitro* binding site selection revealed several features specific to IRF-4. IRF-4 preferentially bound to the sequences containing tandem repeats of 5′-GAAA-3′, which in most cases are flanked by CpC. Although IRF-4 exhibited similar preferences to the SAAB1 and GBP-derived ISRE in the EMSA, our recent fluorescent anisotropy measurements and calorimetric studies clearly demonstrated the IRF-4 preference for the former; the K_d value to the CCGAAA was ~0.3 μM, whereas the GBP-derived GGGAAA was ~4 μM (23, C. Kojima *et al.*, unpublished results).

A similar binding-selection study was reported previously for IRF-1 and IRF-2, and the selected common sequence was 5′-G(A)AAA G/C T/G GAAA G/C T/C-3′ (24). This sequence contains two copies of the core sequence 5′-GAAA-3′, with varied spacer sequence lengths. Although the tandem repeat of the 5′-GAAA-3′core sequence is the same, IRF-4 requires a more stringent spacer length as well as the sequence. In this regard, IRF-1 is quite tolerant to variations in the recognition sequences, which partly explains its wide variety of biological functions. Fine-tuning of the target gene responses by recognition sequence variation was also reported for other members of the IRF family. For example, IRF-3 binds to 5′-GAAA(C/G)(C/G)GAAAN(T/C)-3′, whereas IRF-7 binds to 5′-GAA(A/T)N(C/T)GAAAN(T/C)-3′ (25). IRF-3 is sensitive to the replacement of a single nucleotide within the GAAA core sequence, whereas IRF-7 has a wider recognition capacity. Such differences in the target sequence preference may lead to the exclusive primary induction of IFN-β by IRF-3 and the subsequent continuous expression of IFN-α gene family members by IRF-7, in the host defense system against viral infection (26, 27). It thus may be possible to consider that a particular set of genes bearing IRF-4-SAAB or related sequences are regulated by the concerted actions of IRF-1 and IRF-4 in immune cells.

With the knowledge accumulated to date, it is possible to predict the genome-wide distribution of transcription factor-binding sites *in silico*. We could actually find sequences related to IRF-4–SAAB within the promoter regions of several genes (data not shown). Among them, we demonstrated that two IRF-4–SAAB-related sequences, found in the promoter region of the human TRAIL gene, were necessary for the transactivation by IRF-1. Importantly, IRF-4 dominantly controlled the TRAIL promoter activity over the action of IRF-1. Sequential deletion analyses of IRF-4 revealed that aa 1–129, corresponding to the DBD, were sufficient to repress the IRF-1-dependent transactivation (Fig. 4). This result is consistent with the previous study demonstrating that an IRF-4 mutant, consisting of only the DBD, blocked IFN-α/β- and IRF-1-mediated activation (28). Interestingly, we could not detect the dominant action of IRF-4 over IRF-1 in embryonic caricinoma cells, such as P19 (data not shown), suggesting that the action of IRF-4 may be cell-type specific, even though it can be successfully expressed by transfection. It is also interesting to note that IRF-2, a well-known transcriptional repressor on ISRE, does not show this activity on either the SAAB1 or TRAIL promoter. Although the repressive activity of IRF-2 and IRF-4 was previously demonstrated on the ISREs of the IFN-β and H-2Ld promoters (7), we consider SAAB to be the first ISRE to be negatively regulated by IRF-4, but not IRF-2.

IRF-4 also seems to regulate the expression of the DCIR gene (29). DCIR, also called C-type lectin superfamily 6

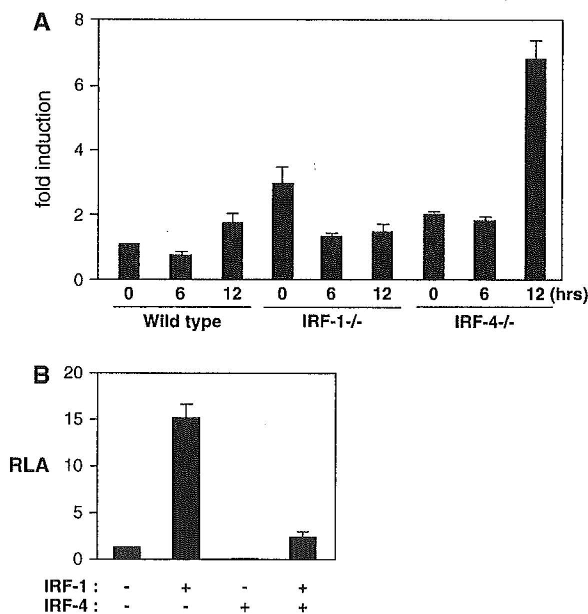

Fig. 7. Transcriptional regulation of DCIR by IRF-1 and IRF-4. (A) Splenic T cells were prepared and treated with Con A for 0, 6 and 12 h, and the quantities of DCIR mRNA were determined by real-time PCR. The results shown are the average of three independent amplifications from the same samples with standard deviation. (B) The $SAAB_{DCIR}$ luciferase activity was determined 48 h after transfection of the reporter construct together with the combination of IRF-1 and IRF-4 cDNAs. The results shown are the average of three independent experiments with standard deviation.

(CLECSF6) (30) or lectin-like immunoreceptor (31), is a transmembrane protein containing an extracellular lectin-like domain and an intracellular immunoreceptor tyrosine-based inhibitory motif (32). DCIR mRNA is expressed strongly in peripheral blood leukocytes, with moderate quantities in the spleen, lymph nodes and bone marrow, and at very low levels in the thymus (29). Although purified blood T cells did not express DCIR mRNA, we observed the weak but reproducible induction of DCIR in splenic T cells by Con A treatment. This induction was dependent on IRF-1, since no induction was observed in IRF-1-deficient T cells. In IRF-1-deficinent splenocytes, it rather seems that DCIR was up-regulated at basal level, but repressed after the Con A treatment. It is possible that IRF-4 induced by Con A is involved in this repression (6). Indeed, IRF-4 seemed to repress the induced expression of DCIR, because the knockout of IRF-4 resulted in the augmentation of DCIR induction by Con A treatment. It is also possible that IRF-4 competitively represses IRF-1 and potentially other activators, including IRFs under certain physiological conditions. Since IRF-4 is exclusively expressed in the $CD11b^{high}$ $CD8\alpha^{-}$ dendritic subset, but not in the $CD11b^{low}$ $CD8\alpha^{+}$ dendritic subset (14), the active repression of DCIR by IRF-4 in the former subset would be involved in the development of $CD11b^{high}$ $CD8\alpha^{-}$ dendritic cells.

IRF-4 is unique among the IRF family members because it is not induced by IFN, but by antigen stimuli. Further research to investigate the role of IRF-4 in immune cells, particularly in terms of its ability to bind the IRF-4–SAAB sequence, may reveal the regulatory nature of IRF-4 in the IFN system.

Acknowledgements

We thank A. Koda, H. Ichinose and M. Miyazaki for encouragement. We are also grateful to B. Mark Evers (University of Texas Medical Branch) for kindly providing the 5′-deletion hTRAIL promoter constructs and the Center for Frontier Life Sciences, Nagasaki University, for sequencing devices and animal breeding. This work was supported by a grant-in-aid and by the 21st Century Center of Excellence Program of Nagasaki University from the Ministry of Education, Culture, Sports, Science, and Technology, Japan.

Abbreviations

aa	amino acids
DBD	DNA-binding domain
DCIR	dendritic cell immunoreceptor
DTT	dithiothreitol
GBP	guanine-binding protein gene
hIRF	human IFN regulatory factor
IAD	IRF association domain
IRF	IFN regulatory factor
PMSF	phenylmethylsulfonylfluoride
SAAB	selected and amplified binding site

References

1 Nguyen, H., Hiscott, J. and Pitha, P. M. 1997. The growing family of IRF transcription factors. *Cytokine Growth Factor Rev.* 8:293.
2 Mamane, Y., Heylbroeck, C., Genin, P. *et al.* 1999. Interferon regulatory factors: the next generation. *Gene* 237:1.
3 Taniguchi, T., Ogasawara, K., Takaoka, A. and Tanaka, N. 2001. IRF family of transcription factors as regulators of host defense. *Annu. Rev. Immunol.* 19:623.
4 Stark, G. R., Kerr, I. M., Williams, B. R. G., Silverman, R. H. and Schreiber, R. D. 1998. How cells respond to interferons. *Annu. Rev. Biochem.* 67:227.
5 Eisenbeis, C. F., Singh, H. and Storb U. 1995. Pip, a novel IRF family member, is a lymphoid-specific, PU.1-dependent transcriptional activator. *Genes Dev.* 9:1377.
6 Matsuyama, T., Grossman, A., Mittrucker, H. W. *et al.* 1995. Molecular cloning of LSIRF, a lymphoid-specific member of the interferon regulatory factor family that binds the interferon-stimulated response element (ISRE). *Nucleic Acids Res.* 23:2127.
7 Yamagata, T., Nishida, J., Tanaka, T. *et al.* 1996. A novel interferon regulatory factor family transcription factor, ICSAT/Pip/LSIRF, that negatively regulates the activity of interferon-regulated genes. *Mol. Cell. Biol.* 16:1283.
8 Marecki, S., Atchinson, M. L. and Fenton M. J. 1999. Differential expression and distinct functions of interferon regulatory factor 4 (IRF4) and interferon consensus sequence binding protein (ICSBP) in macrophages. *J. Immunol.* 163:2713.
9 Ahn, J. H., Lee, Y., Jeon, C. J. *et al.* 2002. Identification of the genes differentially expressed in human dendritic cell subsets by cDNA subtraction and microarray analysis. *Blood* 100:1742.
10 Mittrucker, H. W., Matsuyama, T., Grossman, A. *et al.* 1997. Requirement for the transcription factor LSIRF/IRF4 for mature B and T lymphocyte function. *Science* 275:540.
11 Rengarajan, J., Mowen, K. A., McBride, K. D., Smith, E. D., Singh, H. and Glimcher, L. H. 2002. Interferon regulatory factor 4 (IRF4) interacts with NFATc2 to modulate interleukin 4 gene expression. *J. Exp. Med.* 195:1003.
12 Lohoff, M., Mittrucker, H. W., Stefan, P. *et al.* 2002. Dysregulated T helper cell differentiation in the absence of interferon regulatory factor 4. *Proc. Natl Acad. Sci. USA* 99:11808.
13 Tominaga, N., Ohkusu-Tsukada, K., Udono, H., Abe, R., Matsuyama, T. and Yui, K. 2003. Development of Th1 and not Th2 immune responses in mice lacking IFN-regulatory factor-4. *Int. Immunol.* 15:1.
14 Suzuki, S., Honma, K., Matsuyama, T. *et al.* 2004. Critical roles of interferon regulatory factor-4 in $CD11b^{high}$ $CD8\alpha^{-}$ dendritic cell development. *Proc. Natl Acad. Sci. USA*, 101:8981.
15 Nagulapalli, S. and Atchison, M. L. 1998. Transcription factor Pip can enhance DNA binding by E47, leading to transcriptional synergy involving multiple protein domains. *Mol. Cell. Biol.* 18:4639.
16 Gupta, S., Jiang, M., Anthony, A. and Pernis, A. B. 1999. Lineage-specific modulation of interleukin 4 signaling by interferon regulatory factor 4. *J. Exp. Med.* 191:1281.
17 Blackwell, T. K. and Weintraub, H. 1990. Differences and similarities in DNA-binding preferences of MyoD and E2A protein complexes revealed by binding site selection. *Science* 250:1104.
18 Wang, Q., Ji, Y., Wang, X. and Evers, M. 2000. Isolation and molecular characterization of the 5′-upstream region of the human TRAIL gene. *Biochem. Biophys. Res. Commun.* 276:466.
19 Imanishi, D., Yamamoto, K., Tsushima, H. *et al.* 2000. Identification of a novel cytokine response element in the human IFN regulatory factor-1 gene promoter. *J. Immunol.* 165:3907.
20 Schreiber, E., Matthias, P., Muller, M. M. and Schaffner, W. 1989. Rapid detection of octamer binding proteins with 'mini-extracts,' prepared from a small number of cells. *Nucleic Acids Res.* 17:6419.
21 Uegaki, K., Shirakawa, M., Fujita, T., Taniguchi, T. and Kyogoku, Y. 1993. Characterization of the DNA binding domain of the mouse IRF-2 protein. *Protein Eng.* 6:195.
22 Butler, J. E. F. and Kadonaga, J. T. 2002. The RNA polymerase II core promoter: a key component in the regulation of gene expression. *Genes Dev.* 16:2583.
23 Ishizaki, I., Nomura, M., Yamamoto, K., Matsuyama, T., Mishima, M. and Kojima, C. 2004. Solution of NMR study of DNA recognition mechanism of IRF-4 protein. *Nucleic Acids Symp. Ser.* 48:105.
24 Tanaka, N., Kawakami, T. and Taniguchi, T. 1993. Recognition DNA sequences of interferon regulatory factor 1 (IRF-1) and IRF-2, regulators of cell growth and the interferon system. *Mol. Cell. Biol.* 13:4531.
25 Lin, R., Genin, P., Mamane, Y. and Hiscott, J. 2000. Selective DNA binding and association with the CREB binding protein coactivator contribute to differential activation of alpha/beta interferon

genes by interferon regulatory factors 3 and 7. *Mol. Cell. Biol.* 20:6342.

26 Au, W. C., Moore, P. A., LaFleur, D. W., Tombal, B. and Pitha, P. M. 1998. Characterization of the interferon regulatory factor-7 and its potential role in the transcription activation of interferon A genes. *J. Biol. Chem.* 273:29210.

27 Nakaya, T., Sato, M., Hata, N. *et al.* 2001. Gene induction pathways mediated by distinct IRFs during viral infection. *Biochem. Biophys. Res. Commun.* 283:1150.

28 Taki, S., Sato, T., Ogasawara, K. *et al.* 1997. Multistage regulation of Th1-type immune responses by the transcription factor IRF-1. *Immunity* 6:673.

29 Bates, E. E., Fournier, N., Garcia, E. *et al.* 1999. APCs express DCIR, a novel C-type lectin surface receptor containing an immunoreceptor tyrosine-based inhibitory motif. *J. Immunol.* 163:1973.

30 Richard, M., Veilleux, P., Rouleau, M., Paquin, R. and Beaulieu, A. D. 2002. The expression pattern of the ITIM-bearing lectin CLECSF6 in neutrophils suggests a key role in the control of inammation. *J. Leukoc. Biol.* 71:871.

31 Huang, X., Yuan, Z., Chen, G. *et al.* 2001. Cloning and characterization of a novel ITIM containing lectin-like immunoreceptor LLIR and its two transmembrane region deletion variants. *Biochem. Biophys. Res. Commun.* 281:131.

32 Kanazawa, N., Okazaki, T., Nishimura, H., Tashiro, K., Inaba, K. and Miyachi, Y. 2002. DCIR acts as an inhibitory receptor depending on its immunoreceptor tyrosine-based inhibitory motif. *J. Investig. Dermatol.* 118:261.

© 2005 Oxford University Press
Nucleic Acids Symposium Series No. 49 49–50

Solution structure of a small-molecular ligand complexed with CAG trinucleotide repeat DNA

Kazuhiko Nakatani[1,2], Shinya Hagihara[1], Yuki Goto[1], Akio Kobori[1], Masaki Hagihara[1], Gosuke Hayashi[1], Motoki Kyo[3], Makoto Nomura[4], Masaki Mishima[4] andChojiro Kojima[4]

[1]Graduate School of Engineering, Kyoto University, Kyoto 618-8510, Japan, [2]PRESTO (JST), [3]Toyobo Co. Ltd., Tsuruga, Fukui 914-0047, Japan and [4]Graduate School of Biological Science, Nara Institute of Science and Technology, Nara 630-0192, Japan

ABSTRACT

NMR structure of the first identified ligand, naphthyridine–azaquinolone (NA), complexed with the CAG-CAG triad is reported. The determined structure revealed the invasive ligands binding to the A-A mismatch and flanking G-C base pairs, causing the widowed cytosines to flip out from π-stack. Hydrogen-bond pairs between NA and DNA, naphthyridine-guanine and azaquinolone-adenine, are well stacked in the right-handed DNA helix, showing structural mimicry of Watson–Crick base pairing. This is the first observation that the small molecular ligand induced the base flipping of the nucleotide base in the Watson-Crick base pair.

INTRODUCTION

Trinucleotide repeat expansions in genomic DNA are the molecular basis of a growing number of hereditary diseases. The characteristic feature of these diseases is a phenomenon termed as anticipation. A longer repeat length would lead to the increasing disease severity and decreasing age at onset in succeeding generations. The mechanism of $(CAG)_n$, $(CTG)_n$, and $(CGG)_n$ repeats expansion is considered to correlate to the increased stability of the metastable hairpin form consisting of CXG/CXG triads involving X-X mismatches. Ligands binding to $(CXG)_n$ repeats would be important molecular probes for determining the repeat length and the repeat expansion mechanism. Here we show the solution structure of the first identified ligand, naphthyridine–azaquinolone (NA), complexed with the CAG/CAG triad.

RESULTS AND DISCUSSION

Complex formation between NA and an 11-mer DNA duplex containing CAG-CAG was monitored by ^1H one-dimensional imino protón spectra while NA was titrated (Figure 1). Signals from free DNA and the NA-DNA complex were observed separately on a slow-exchange

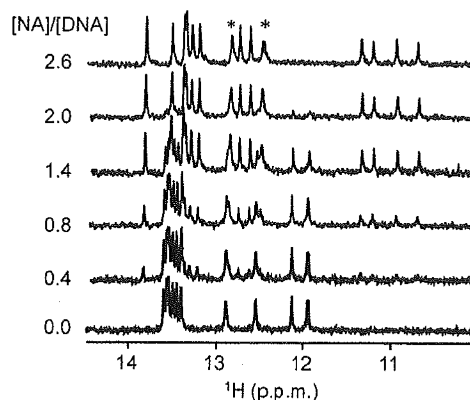

Figure 1. One dimensional 1H spectra of 0.1 mM unlabeled 11-mer CAG-CAG at different NA concentrations at 275 K. The concentration ratios of NA to DNA are shown at left.

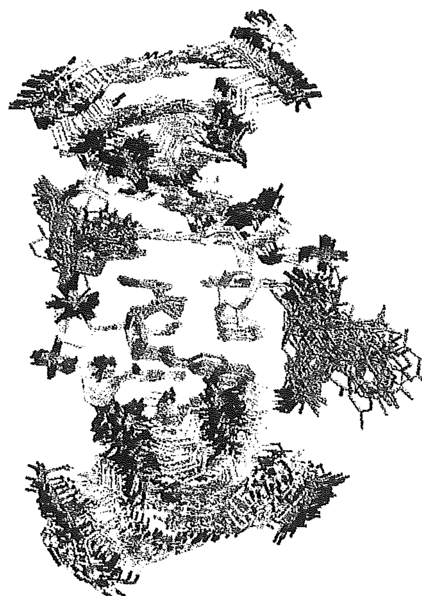

Figure 2. NMR structures of NA-CAG/CAG complex. 30 complex structures are superimposed focusing on A6, G7, A17, G18, NA1, and NA2 residues.

timescale. The stoichiometry was easily and unambiguously determined to be 2:1 (NA:DNA), and no intermediate was observed. NMR spectra of the NA-DNA complex were recorded using $^{13}C^{15}N$-labelled DNA. The determined solution structure of the complex revealed the invasive ligands binding to the A-A mismatch and flanking G-C base pairs, causing the widowed cytosines to flip out from π-stack (Figure 2). Hydrogen-bond pairs between NA and DNA, naphthyridine-guanine and azaquinolone-adenine, are well stacked in the right-handed DNA helix, showing structural mimicry of Watson–Crick base pairing (Figure 3). This is the first observation that the small molecular ligand induced the base flipping of the nucleotide base in the Watson-Crick base pair.

Strong NA binding to the CAG-CAG triad induced formation of the NA-bound hairpin form in long $(CAG)_n$ repeats. Given the ability of NA to bind CAG repeats, a sensor in which NA was immobilized on an SPR chip was created, and its utility was assessed for diagnosis of the CAG repeat length by SPR analysis. SPR analyses of the binding of $d(CAG)_{10}$, $d(CAG)_{20}$ and $d(CAG)_{30}$ to the immobilized NA dimmer showed that signal intensities increased with repeat length. The SPR intensities of $d(CAG)_{30}$ were stronger than those of $d(CAG)_{10}$ and $d(CAG)_{20}$ at a wide range of DNA concentrations (1), suggesting that it may be possible to use the NA-immobilized SPR sensor for the rapid diagnosis of CAG repeat length.

CONCLUSION

NA-CAG-CAG complex structure determined by NMR provides the theoretical basis to design and optimize the CXG triad binding ligands. In fact, the similar structural feature has been found in the complex of naphytiridine-dimer with CGG triad (2). Currently, there is no effective therapeutic agent for treating diseases caused by triplet repeat expansion. The discovery of the small-molecular ligand NA, which binds with high affinity to repeat sites, may be a substantial substantial step toward developing effective therapeutic agents for these hereditary diseases.

ACKNOWLEDGMENTS

This work was partially supported by a Grant in Aid for Scientific Research (A) from the Japan Society for the Promotion of Science to K.N., Health and Labour Sciences Research Grants for Research on Advanced Medical Technology from the Ministry of Health, Labour and Welfare to K.N. and C.K., and CREAST, Japan Science and Technology Agency to K.N.

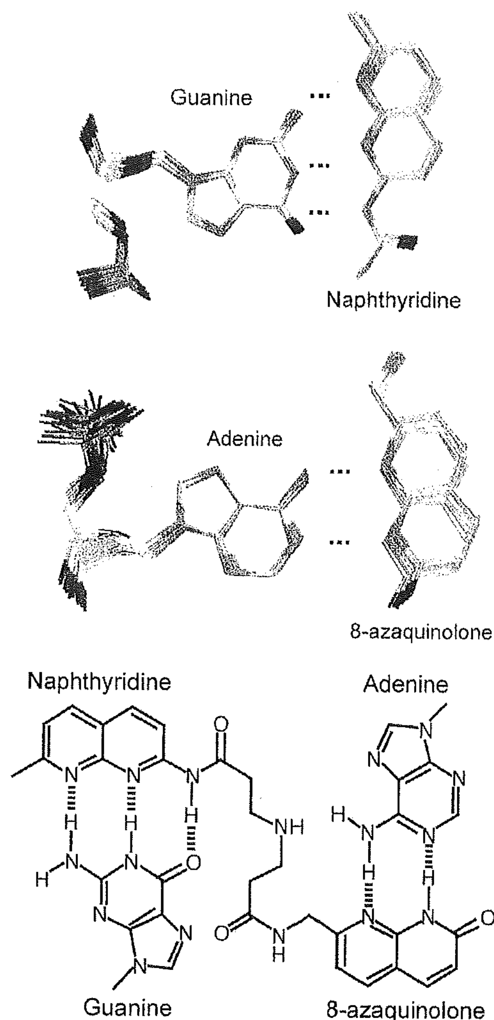

Figure 3. Superimposed NMR structures for the hydrogen bonding between guanine and naphthyridine (top) and adenine and 8-azaquinolone (middle). Naphthyridine chromophore is complementary in hydrogen bonding surface to guanine, whereas 8-azaquinolone is complementary to adenine (bottom).

REFERENCES

1. Nakatani, K., Hagihara, S., Goto, Y., Kobori, A., Hagihara, M., Hayashi, G., Kyo, M., Nomura, M., Mishima, M. and Kojima, C. (2005) *Nature Chemical Biology*, **1**, 39-43.
2. Nomura, M., Hagihara, S., Goto, Y., Nakatani, K. and Kojima, C. (2005) *Nucleic Acid Res. Suppl.*, this issue.

© 2005 Oxford University Press

Nucleic Acids Symposium Series No. 49 **51–52**

NMR spectroscopic analyses of functional nucleic acids-metal interaction and their solution structure analyses

Yoshiyuki Tanaka[1], Hiroshi Yamaguchi[1], Shuji Oda[1], Chojiro Kojima[2], Akira Ono[3], Kazunari Taira[4,5] and Yoshinori Kondo[1]

[1]Graduate School of Pharmaceutical Sciences, Tohoku University, Aobayama, Aoba-ku, Sendai 980-8578, Japan, [2]Graduate School of Biological Sciences, Nara Institute of Science and Technology, Japan, [3]Department of Applied Chemistry, Faculty of Engineering, Kanagawa University, Japan, [4]Department of Chemistry and Biotechnology, School of Engineering, The University of Tokyo, Japan and [5]Gene Function Research Center, AIST, Japan

ABSTRACT

We have studied complexations of functional nucleic acids and metal ions, by means of NMR spectroscopy. In the case of hammerhead ribozymes, they have a metal ion-binding motif in their core sequences. Upon the metallation of N7 of a guanosine in an RNA duplex modelled after hammerhead ribozymes, 20 ppm higher field shift of N7 was observed in 1-dimensional (1D) ^{15}N NMR spectra. It was found that metal ion binding to nucleobases were detectable with ^{15}N NMR spectroscopy.

INTRODUCTION

Biologically active RNA molecules utilize metal ions to fold into specific conformation or to form a catalytic center. In order to reveal their mechanisms of actions, it is important to establish methodologies for detecting metallations of nucleic acids. In the conserved core region of hammerhead ribozymes, there is a metal ion-binding motif (the A9/G10.1 site) in which N7 of guanosine (G10.1) is metallated (1-3). Therefore, the A9/G10.1 motif is suitable for establishing methodologies for the detection of nucleobase metallations. Furthermore, in order to understand the mechanism of hammerhead ribozymes, it is becoming important whether the metal ion at this motif is a catalytic center or just a structural constituent (4-6). Therefore, it is obviously important to study the interaction between metal ions and the metal ion-binding motif.

RESULTS AND DISCUSSION

We chemically synthesized series of RNA oligomers as shown below.

GA10: r(GGA*CGA*__*G*__UCC)
UGAA10: r(GGA*UGAA*UCC)

where the metallated guanosine (G10.1) and corresponding residues are in bold characters. In the case of GA10, we also synthesized stable isotope labelled RNA oligomers.

r(GGACGAGUCC) r(GGACGAGUCC)
r(GGACGAGUCC) r(GGACGAGUCC)

where underlined residues are uniformly ^{15}N- and ^{13}C-labeled guanosine residues. By using these RNA oligomers, titration experiments were performed (7-10). It was found that the chemical shift of N7 of guanosine was suitable for the detection of a nucleobase metallation, since the large chemical shift change was observed for N7(G10.1) (Table 1). More importantly, ^{15}N NMR spectroscopy (chemical shifts or *J*-coupling) seems to be applicable for other metal-nucleic acid complexes, such as mercury mediated T-T base-pair (T-Hg-T) (11).

We also examined roles of this metal ion at the motif, using an RNA oligomer with a motif of hammerhead mutants. The Mg^{2+}-titration for this mutant motif (G10.1-C11.1 to A10.1-U11.1) revealed that its affinity to Mg^{2+} was drastically reduced, although the ribozyme with this mutant motif is known to retain enzymatic activities. This observation suggests that the metal ion at the A9/G10.1 site is not a catalytic center of hammerhead ribozymes.

REFERENCES

1. Pley, H. W., Flaherty, K. M. and McKay, D. B. (1994) *Nature*, **372**, 68-74.
2. Scott, W. G., Murray, J. B., Arnold, J. R., Stoddard, B. L. and Klug, A. (1996) *Science*, **274**, 2065-2069.
3. Murray, J. B., Terwey, D. P., Maloney, L., Karpeisky, A.; Usman, N., Beigelman, L. and Scott, W. G. (1998) *Cell*, **92**, 665-673.
4. Wang, S., Karbstein, K., Peracchi, A., Beigelman, L. and Herschlag, D. Biochemistry 1999, 38, 14363-14378.
5. Yoshinari, K. and Taira, K. (2000) *Nucleic Acids Res.*, **28**, 1730-1742.

Table 1 Summary of the ^{15}N, ^{13}C and ^{1}H NMR data

Metal ligand	Metal	Residue	δ(N7)[a] / ppm	δ(C8)[a] / ppm	δ(H8)[a] / ppm	$^{1}J_{N-M(II)}$[b] / Hz	Ref.
GA10[c]	Cd^{2+}	G10.1	-19.6 (3.0 eq)	+2.3 (2.5eq)	+0.38 (4.5eq)	not detected	7-9
GA10[c]	Mg^{2+}	G10.1	N.D.	+0.5 (1.0eq)	+0.12 (4.5eq)	n.a.	8-10
GA10[c]	$[Co(NH_3)_6]^{3+}$	G10.1	N.D.	< +0.1 (1.0eq)	+0.25 (1.5eq)	n.a.	8,9
GA10[c]	Na^{+}	G10.1	N.D.	< +0.1 (230 mM)[d]	+0.12 (800 mM)[d]	n.a.	8,9
RNA decamer[e]	Cd^{2+}	G10.1	~ -20 (6.0 eq)	N.D.	N.D.	N.D.	12
RNA decamer[e]	Zn^{2+}	G10.1	~ -20 (4.0 eq)	N.D.	N.D.	n.a.	12
RNA decamer[e]	Mg^{2+}	G10.1	-6.5 (10.0 eq)	N.D.	N.D.	n.a.	12
RNA decamer[e]	$[Co(NH_3)_6]^{3+}$	G10.1	< -1 (6.0 eq)	N.D.	N.D.	n.a.	12
Inosine[f]	Zn^{2+}	n.a.	-15.2 (0.7 eq)	N.D.	N.D.	n.a.	13
Inosine[f]	Hg^{2+}	n.a.	-4.8 (0.75 eq)	N.D.	N.D.	not detected	13
Guanosine[f]	Zn^{2+}	n.a.	-20.1 (1.0 eq)	N.D.	N.D.	n.a.	14
Guanosine[f]	Hg^{2+}	n.a.	-20.5 (1.0 eq)	N.D.	N.D.	N.D.	14
Guanosine (calc.)[g]	Zn^{2+}	n.a.	-14.8	N.D.	N.D.	-36.5[h]	15
Guanosine (calc.)[g]	Mg^{2+}	n.a.	-15.3	N.D.	N.D.	5.6[h]	15
DNA dodecamer[i]	Zn^{2+}	G4	N.D.	+2.5 (8.0eq)	+0.20 (8.0eq)	N.D.	16
DNA dodecamer[i]	Zn^{2+}	G3	N.D.	+1.5 (8.0eq)	+0.05 (8.0eq)	N.D.	16
d(TGGT)	$Pt(en)Cl_2$[j]	G3	N.D.	+1.1 (1.0eq)	+1.04 (1.0eq)	N.D.	17
d(TGGT)	$Pt(en)Cl_2$[j]	G2	N.D.	+0.2 (1.0eq)	+0.26 (1.0eq)	N.D.	17
UGAA10[k]	Mg^{2+}	A10.1	N.D.	N.D.	< +0.01 (1.0eq)	n.a.	8,9

not detected: *J*-coupling was not detected, although trials for its detection have been made. n.a.: not applicable. N.D.: not determined. [a] Chemical shift perturbations from the non-metalated state. Negative and positive values indicate higher- and lower-field shifts, respectively. The numbers in parentheses beside the perturbation values indicate the molar ratios of $[CdCl_2]$/[motif or nucleoside]. [b] *J*-coupling between metalated nitrogens (^{15}N) and metal ions (I=1/2), such as ^{113}Cd and ^{199}Hg. [c] r(GGACGA**G**UCC)$_2$. [d] Chemical shift perturbations from basal solution (40 mM Na^{+}). [e] RNA decamer: r(CGGUUGA**G**GC) r(GCCGAAACCG) The metal cation binding motif is underlined, and the metalated guanosine is shown in boldface. [f] Titration experiments were performed in dimethyl sulfoxide (DMSO). [g] Theoretical values from molecular orbital calculations. [h] The quadrupole moments of ^{67}Zn and ^{25}Mg are so large that experimental *J*-coupling values are not available currently. [i] DNA dodecamer: d(AT**GG**GTACCCAT)$_2$ [j] One $Pt(en)Cl_2$ (en = ethylenediamine) forms two covalent bonds with the two successive guanosines of d(T**GG**T). [k] r(GGAUGA**A**UCC)$_2$ [l] r(GGAGGACUCC)$_2$

6. O'rear, J. L., Wang, S., Feig, A. L., Beigelman, L., Uhlenbeck, O. C. and Herschlag, D. (2001) RNA, **7**, 537-545.
7. Tanaka, Y., Kojima, C., Morita, E. H., Kasai, Y., Yamasaki, K., Ono, A., Kainosho, M. and Taira, K. (2002) *J. Am. Chem. Soc.*, **124**, 4595-4601.
8. Tanaka, Y., Kasai, Y., Mochizuki, S., Wakisaka, A., Morita, E. H., Kojima, C., Toyozawa, A., Kondo, Y., Taki, M., Takagi, Y., Inoue, A., Yamasaki K. and Taira, K. (2004) *J. Am. Chem. Soc.*, **126**, 744-752.
9. Tanaka, Y. and Taira, K. (2005) *Chem. Commun.*, 2069-2079.
10. Tanaka, Y., Morita, E. H., Hayashi, H., Kasai, Y., Tanaka, T. and Taira, K. (2000) *J. Am. Chem. Soc.*, **122**, 11303-11310.
11. Ono, A., Togashi, H. (2004) *Angew. Chem. Int. Ed.*, **43**, 4300-4302.
12. Wang, G., Gaffney B. L. and Jones R. A. (2004) *J. Am. Chem. Soc.*, **126**, 8908-8909.
13. Buchanan, G. W. and Bell, M. J. (1983) *Can. J. Chem.*, **61**, 2445-2448.
14. Buchanan, G. W. and Stothers, J. B. (1982) *Can. J. Chem.*, **60**, 787-791.
15. Sychrovsky, V., Sponer, J. and Hobza, P. (2004) *J. Am. Chem. Soc.*, **126**, 663-672.
16. Jia, X., Zon G. and Marzilli, L. G. (1991) *Inorg. Chem.*, **30**, 228-239.
17. Mukundan, Jr., S., Xu, Y., Zon G. and Marzilli, L. G. (1991) *J. Am. Chem. Soc.*, **113**, 3021-3027.

© 2005 Oxford University Press
Nucleic Acids Symposium Series No. 49 199–200

Spectroscopic analyses of DNA duplexes in the presence of mercury ions

Hiroshi Yamaguchi[1], Shuji Oda[1], Chojiro Kojima[2], Akira Ono[3], Yoshinori Kondo[1] and Yoshiyuki Tanaka[1]

[1]Graduate School of Pharmaceutical Sciences, Tohoku University, Aobayama, Aoba-ku, Sendai, Miyagi 980-8578, Japan, [2]Graduate School of Biological Science, Nara Institute of Science and Technology, Ikoma, Nara 630-0101, Japan and [3]Department of Applied Chemistry, Faculty of Engineering, Kanagawa University, Kanagawa-ku Yokohama, Kanagawa 221-8686, Japan

ABSTRACT

The DNA duplex with tandem T•T mismatches in the presence of Hg(II) has been studied by NMR spectroscopy. For this study, we synthesized decamer duplex with two successive T•T mismatches (TT10). From two-dimensional (2D) ^{1}H-^{1}H NOESY spectrum of TT10 in complex with Hg(II), we were able to trace sequential NOE walks between base protons and anomeric protons (H1'), and assigned all of them. Based on these assignments and NOESY spectra, we could assigned all the non-exchangeable protons of TT10 in the presence of Hg(II).

INTRODUCTION

Watson-Crick base pair is essential for the stability and specificity of duplex formation. Additional stable and selective base pairs would increase the capacity of DNA for information storage and might allow generation of DNAs with novel function. As one of efforts to develop such an unnatural base pair, a strategy that hydrogen bonding interactions are replaced by metal-dependent pairing of two nucleobases have recently reported. Most of this type of base pair had developed by artificial nucleobase (1-10). Recently, it was reported that thymine-thymine (T•T) mismatches in a duplex form a stable Hg(II)-mediated T•T base pair (11). Using DNA oligomer include tandem T•T mismatches, highly selective and sensitive mercury(II) sensor has developed (12). Originally, it was reported that the Hg(II)-mediated T•T base pair had been suggested by pH titration, UV, CD and NMR spectroscopic methods (13-19). However, its definitive structure has not been elucidated, to date. For this reason, T•T mismatches became interesting target for structural studies again. We have already reported resonance assignments of non-exchangeable protons in a Hg(II)-free state DNA duplex including T•T mismatches, by using NMR spectroscopy (20). In this study, we assigned non-exchangeable proton resonances in a DNA oligomer with T•T mismatches in the presence of Hg(II), as well as its exchangeable proton resonances in the absence of Hg(II).

MATERIALS AND METHODS

Two DNA decamers of 5'-CGCGTTGTCC-3' and 5'-GGACTTCGCG-3' were synthesized by the phosphoramidite method on an automated DNA/RNA synthesizer (ABI model 392). Each oligomer was purified by C18 reversed-phase column (COSMOSIL 5C18-AR-300, nakalai tesque, Japan) on HPLC system, with a linear gradient of acetonitrile. For the exchange of counter ions, each oligomer was adsorbed onto an anion-exchange column (UNO-Q; Pharmacia Biotech, Uppsala, Sweden). The column was washed with more than 10 column volumes of MILLI-Q water (MILLIPORE, USA) to wash out triethylammonium ions. The oligomer was eluted with 2M NaCl to make Na^+ the counter ion. Finally, excess NaCl was removed by a Gel filtration column (TSK-GEL G3000PW; TOSO, Japan) with MILLI-Q water as the mobile phase. The final solution contained only the oligomer and the counter ion (Na^+ ion). Each oligomer was quantitated by UV absorbance at 260 nm after digestion by nuclease P1.

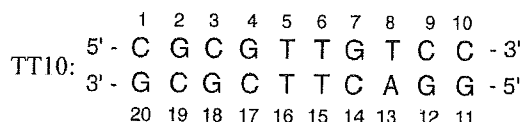

Scheme 1

In order to prepare NMR solutions of a Hg(II)-bound DNA oligomer, we made solutions containing 2.0 mM TT10, 40 mM $NaClO_4$ and 4.8 mM $HgClO_4$. Then these solutions were passed through chelating resin (chelex; BIO-RAD, USA), for the removal of trace amount of paramagnetic metal cations and excess Hg(II). Solution conditions for the NMR measurements of a Hg(II)-free DNA oligomer contains 2.0 mM TT10 and 40 mM $NaClO_4$. Two-dimensional (2D) ^{1}H-^{1}H NOESY spectrum were recorded on Bruker DMX500 spectrometer, at 293 K, 8192 * 2048 complex points for a spectral width of 10000 * 10000 Hz (Hg(II)-free state), and on Bruker DMX800 spectrometer, at 293 K, 8192 * 2048 complex points for a spectral width of 8013 * 8013 Hz (Hg(II)-bound state).

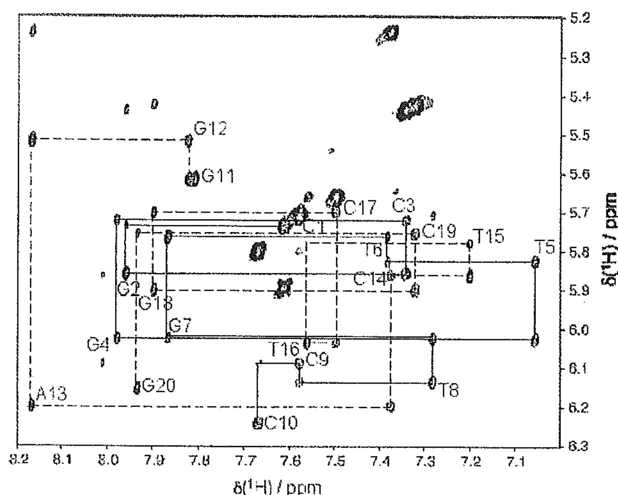

Figure 1. 2D ^{1}H-^{1}H NOESY spectra of TT10 in the presence of Hg(II). The solid and broken lines indicate the sequential NOE walks between H6/H8 and H1' resonances. Intraresidue NOE cross peaks were labeled with their residue numbers. Unlabeled strong NOEs correspond to intraresidue H5-H6 NOE cross peaks of cytidines.

RESULTS AND DISCUSSION

Sequential resonance assignments of TT10 have been carried out in the presence of Hg(II). Figure 1 shows sequential NOE connectivities between base protons (H6/H8) and anomeric protons (H1') in the NOESY spectrum. As apparently from Figure, sequential NOEs were traceable through the both strands unambiguously. Based on these assignments, we also assigned all the resonances of other non-exchangeable protons. In combination with a DQF-COSY spectrum, we assigned all H2' and H2" protons, stereospecifically. However, we were not able to perform stereospecific assignments of H5' and H5" protons. It should be mentioned that the assignments of all non-exchangeable proton resonances from NOESY spectra were consistent with each other, as well as those from the DQF-COSY spectrum.

Then we measured a 2D NOESY spectrum of Hg(II)-free TT10, as well. From the spectrum, four imino proton resonances observed around 11 ppm were found to be imino protons of T•T mismatches. From NOE connectivities of imino proton resonances, they were assigned except for those at terminal base-pairs.

In conclusion, we unambiguously assigned most of non-exchangeable proton resonances of TT10 in the presence and absence of Hg(II).

REFERENCES

1. Switzer, C., Sinha, S., Kim, P. H. and Heuberger, B. D. (2005) *Angew. Chem. Int. Ed.*, **44**, 1529-1532.
2. Zimmermann, N., Meggers, E. and Schultz, P. G. (2004) Bioorg. Chem., **32**, 13-25.
3. Zhang, L. and Meggers, E. (2005) *J. Am. Chem. Soc.*, **127**, 74-75.
4. Meggers, E., Holland, P. L., Tolman, W. B., Romesberg, F. E. and Schultz, P. G. (2000) *J. Am. Chem. Soc.*, **122**, 10714-10715.
5. Weizman, H. and Tor, Y. (2001) *J. Am. Chem. Soc.*, **123**, 3375-3376.
6. Atwell, S., Meggers, E., Spraggon, G. and Schultz, P. G. (2001) *J. Am. Chem. Soc.*, **123**, 12364-12367.
7. Tanaka, K., Yamada, Y. and Shionoya, M. (2002) *J. Am. Chem. Soc.*, **124**, 8802-8803.
8. Tanaka, K., Tengeiji, A., Kato, T., Toyama, N. and Shionoya, M. (2003) *Science*, **299**, 1212-1213.
9. Zimmermann, N., Meggers, E. and Schultz, P. G. (2002) *J. Am. Chem. Soc.*, **124**, 13684-13685.
10. Tanaka, K., Tengeiji, A., Kato, T., Toyama, N., Shiro, M. and Shionoya, M. (2002) *J. Am. Chem. Soc.*, **124**, 12494-12498.
11. Ono, A. and Miyake, Y. (2003) *Nucleic Acids Res. Suppl.*, **3**, 229-230.
12. Ono, A. and Togashi, H. (2004) *Angew. Chem. Int. Ed.*, **43**, 4300-4302.
13. Yamane, T. and Davidson, N. (1961) *J. Am. Chem. Soc.*, **83**, 2599-2607.
14. Katz, S. (1962) *Nature*, **195**, 997-998.
15. Gruenwedel, D. W. (1994) *Biophys. Chem.*, **52**, 115-123.
16. Gruenwedel, D. W. (1994) *J. Inorg. Biochem.*, **56**, 201-212.
17. Ferreira, R., Ben-zvi, E., Yamane, T.,Vasilevskis, J. and Davidson, N. *Advance in the Chemistry of the Coordination Compounds*, 457-462.
18. Buncel, E., Boone, C., Joly, H., Kumar, R. and Norris, A. R. (1985) *J. Inorg. Biochem.*, 25, 61-73.
19. Katz, S. (1963) *Biochim. Biophys. Acta,* 68, 240-253.
20. Yamaguchi, H., Oda, S., Kondo, Y., Ono, A. and Tanaka, Y. (2004) *Nucleic Acids Symposium Series,* **48**, 113-114.

© 2005 Oxford University Press

Nucleic Acids Symposium Series No. 49 213–214

NMR structural analysis of the G.G mismatch DNA complexed with naphthyridine-dimer

Makoto Nomura[1], Shinya Hagihara[2,3], Yuki Goto[2], Kazuhiko Nakatani[2,3,4] and Chojiro Kojima[1]

[1]Graduate School of Biological Science, Nara Institute of Science and Technology, Nara 630-0101, Japan and [2]Department of Synthetic Chemistry and Biological Chemistry, Graduate School of Engineering, Kyoto University, Kyoto 618-8510, Japan and [3]PRESTO, Japan Science and Technology Agency and [4]The Institute of Scientific and Industrial Research, Osaka University, Osaka 567-0047, Japan

ABSTRACT

Naphthyridine-dimer (ND) specifically recognizes G.G mismatch DNA (Figure 1). However, its detailed recognition mechanism is not clear. Here a DNA oligomer d(CTAACGGAATG) / d(CATTCGGTTAA) complexed with ND was studied by NMR. The stoichiometry of DNA to ND was determined to be 1:2 at NMR concentration (2.5 mM). Proton resonances were completely assigned including H5' and H5" using ^{1}H-^{1}H and ^{1}H-^{13}C 2D spectra of the complex. These spectra showed that four naphthyridine rings are staked in the helix and form hydrogen bonds with the four G residues in CGG / CGG region. These results indicate ND can specifically recognize the CGG / CGG sequence.

INTRODUCTION

For detecting single nucleotide polymorphism (SNP), naphthyridine-dimer (ND) has been developed and characterized as the novel sensor for the surface plasmon resonance (SPR) array (*1, 2*). ND recognizes G.G mismatches, and is applicable to various important sequences which include G.G mismatch such as the G-rich telomeric repeat sequence (*3*). Our resent studies revealed that (CAG)$_n$ triplete repeat sequences which have A.A mismatches are recognized by ND like drug, naphthyridine-azaquinolone (NA) (*4*). From ESI-TOF mass analysis, ND binds d(CTAACGGAATG) / d(CATTCGGTTAA) at two different stoichiometries, DNA:ND = 1:1 and 1:2 (*5*). The 1:2 mode is dominant when six-fold ND is present. The detailed recognition mechanisms and the reason why the stoichiometry is differet are not clear. The other key aspect is the ND linker structure which connects two naphtyridine rings. The modification of the ND linker changes binding characters such as thermo-stability and specificity to G.G mismatch (*6, 7*). Thus, the modification of the linker potentially can control the specificity to CGG / CGG sequence. In this study, using ^{1}H-^{1}H NOESY spectra of ND-DNA complex, the structural aspects of ND-DNA complex were studied to reveal the G.G mismatch recognition mechanism. Especially, the stoichiometry and the linker structure were carefully investigated.

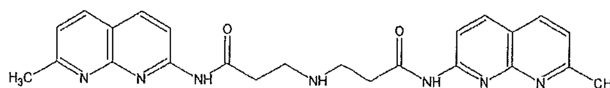

Figure 1. Naphthiridine-dimer (ND). Four nitrogen atoms of naphthiridine rings form hydrogen bonds with imino and amino protons of G. Two amide NH atoms form hydorogen bonds with carboxyl oxygen atoms of G.

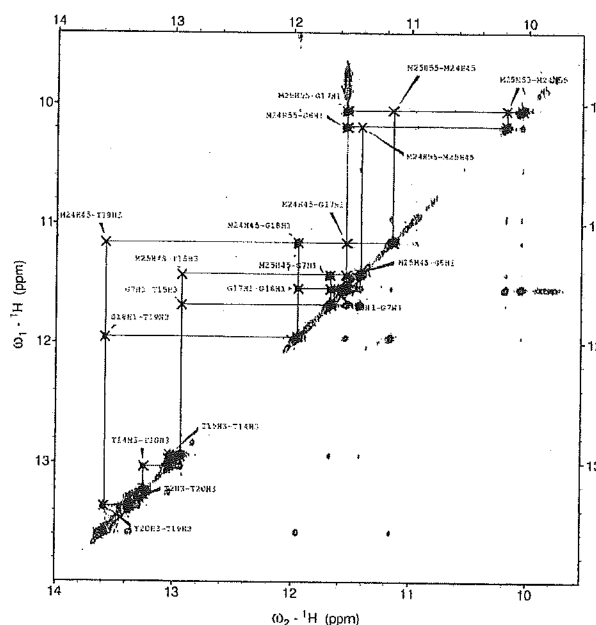

Figure 2. Sequential NOEs of d(CTAACGGAATG) / d(CATTCGGTTAA) complexed with two NDs. Imino protons of nucleic acid bases and four amide protons of NDs are shown in this region.

RESULTS AND DISCUSSION

The ND titration experiments to 2.5 mM d(CTAACGGAATG) / d(CATTCGGTTAA) duplex were carried out monitoring the imino-proton region. The peak